arXiv:0904.4625v1 [q-bio.PE] 29 Apr 2009

Genetic Demixing and Evolutionary Forces in the One-Dimensional Stepping Stone Model

K.S. Korolev,[1,*] Mikkel Avlund,[1,2] Oskar Hallatschek,[1,3] and David R. Nelson[1]

[1]*Department of Physics and FAS Center for Systems Biology, Harvard University, Cambridge, Massachusetts 02138, USA*

[2]*Niels Bohr Institute, University of Copenhagen, Denmark*

[3]*Max Planck Institute for Dynamics and Self-Organization, 37073 Göttingen, Germany*

(Dated: April 29, 2009)

Abstract

We review and extend results for mutation, selection, genetic drift, and migration in a one-dimensional continuous population. The population is described by a continuous limit of the stepping stone model, which leads to the stochastic Fisher-Kolmogorov-Petrovsky-Piscounov equation with additional terms describing mutations. Although the stepping stone model was first proposed for population genetics, it is closely related to "voter models" of interest in nonequilibrium statistical mechanics. The stepping stone model can also be regarded as an approximation to the dynamics of a thin layer of actively growing pioneers at the frontier of a colony of microorganisms undergoing a range expansion on a Petri dish. We find that the population tends to segregate into monoallelic domains. This segregation slows down genetic drift and selection because these two evolutionary forces can only act at the boundaries between the domains; the effects of mutation, however, are not significantly affected by the segregation. Although fixation in the neutral well-mixed (or "zero dimensional") model occurs exponentially in time, it occurs only algebraically fast in the one-dimensional model. If selection is weak, selective sweeps occur exponentially fast in both well-mixed and one-dimensional populations, but the time constants are different. We also find an unusual sublinear increase in the variance of the spatially averaged allele frequency with time. Although we focus on two alleles or variants, q-allele Potts-like models of gene segregation are considered as well. Our analytical results are checked with simulations, and could be tested against recent spatial experiments on range expansions off linear inoculations of Escherichia coli and Saccharomyces cerevisiae.

PACS numbers: 87.23.Kg, 87.23.Cc, 87.18.Hf, 64.60.De

Keywords: stepping stone model, stochastic Fisher-Kolmogorov-Petrovsky-Piscounov equation, selective sweep, voter model, Eden model.

*Electronic address: papers.korolev@gmail.com

I. INTRODUCTION

The quantitative theory of evolution is an important open problem. The theory of evolutionary dynamics is necessary to determine the history of species migrations, and it could shed light on the origin and development of life. Moreover, a better understanding of the evolutionary dynamics could help control epidemics, fight diseases with an evolutionary character such as cancer and acquired immune deficiency syndrome, and guide the engineering of artificial evolution for practical applications.

Most of the current understanding of evolutionary dynamics comes from population genetics, a scientific discipline that studies how evolutionary forces shape the genetic diversity of populations. The majority of theoretical models and experiments in population genetics study only one or a few well-mixed populations, that is populations without spatial structure, where every individual is equally likely to interact with any other individual inside the same population. Microorganisms growing and evolving in a well-mixed liquid culture provide an important example. While nonspatial models are often easier to analyze than spatial ones, they do miss what can be essential features of natural populations.

In nature, organisms often occupy areas that are much larger than the square of the dispersal distance, that is the distance typically traveled by an individual in one generation. This causes two main problems for well-mixed-population models. First, well-mixed-population models underestimate the role of genetic drift (fluctuations due to the discreteness of the number of individuals). The difference arises because the organisms can only interact with their neighbors, and the number of neighbors within the dispersal distance is much smaller than the total number of organisms in the entire population. Second, well-mixed-population models neglect the spatial structure of the population that can be created by external factors or by internal dynamics. Such spatial structures often exist, and, as we show in this paper, they can significantly affect evolutionary processes in the population.

Well-mixed-population models are particularly inadequate when applied to expanding populations. Expansions are very common in biology. Species spread to new territories from the locations where they first evolved. Expansions also occur because of environmental changes such as the global warming and the glacial cycles or due to sudden long distance migrations to new habitats. Even though well-mixed-population models can account for the growing number of individuals (population size), these models do not capture the fact that

the newly settled areas are colonized by the offspring of only a small number of individuals at the expanding front. Since the ancestral population is small, the genetic drift is strong. As a result, neutral genetic diversity decreases with the distance from the origin of the expansion. This reduction in genetic diversity, which is often called "the founder effect" [1], has been observed in humans [2, 3] and many other species. For example, the founder effect in the population waves following the receding glaciers is believed to be responsible for the reduced genetic diversity in high latitude regions compared to equatorial ones [4].

The spreading of Escherichia coli (E. coli) and Saccharomyces cerevisiae (S. cerevisiae) on Petri dishes has been investigated in recent experiments by Hallatschek *et al.* [5]. In these experiments, microbes grown in the dark carried one of two selectively neutral alleles, differing only in a gene encoding for proteins with two distinct fluorescence spectra. Figure 1 shows the expansion of an initially well-mixed $50-50$ population of E. coli into two unoccupied half planes initiated by a razor blade inoculation with cells grown up in liquid culture. The distinctive feature illustrated by the typical experiment in Fig. 1 is that the population does not remain well-mixed; instead, it segregates into well-defined domains. The segregation occurs because the strong genetic drift associated with reduced population size facilitates fixation of one of the two alleles at the front.

Analogous phenomena should also occur in a nonexpanding one-dimensional population because its dynamics is similar to the dynamics of the front of a growing population. The front of a population wave and a literally one-dimensional habitat are not exactly equivalent because the contour of the front undergoes undulations while a one-dimensional habitat has a fixed linear shape. Nevertheless, both are effectively one-dimensional and should deviate from the predictions of well-mixed-population models in similar ways. The advantage of a flat one-dimensional habitat is that it is easier to analyze. In addition, although most species live in effectively two dimensional habitats, a quasi one-dimensional habitat could describe a bank of a river, a sea coast, and a slope of a linear mountain range.

To study the dynamics of a population analytically, we adopt the stepping stone model proposed by Kimura and Weiss [6]. This model considers many well-mixed populations, demes, located on a spatial lattice. Each deme is subject to mutation, selection, genetic drift, and short range migration between neighboring demes. In the limit of weak evolutionary forces and large number of demes, the stepping stone model is equivalent to the continuous models proposed by Wright [7] and Malécot [8] and is described by the stochastic

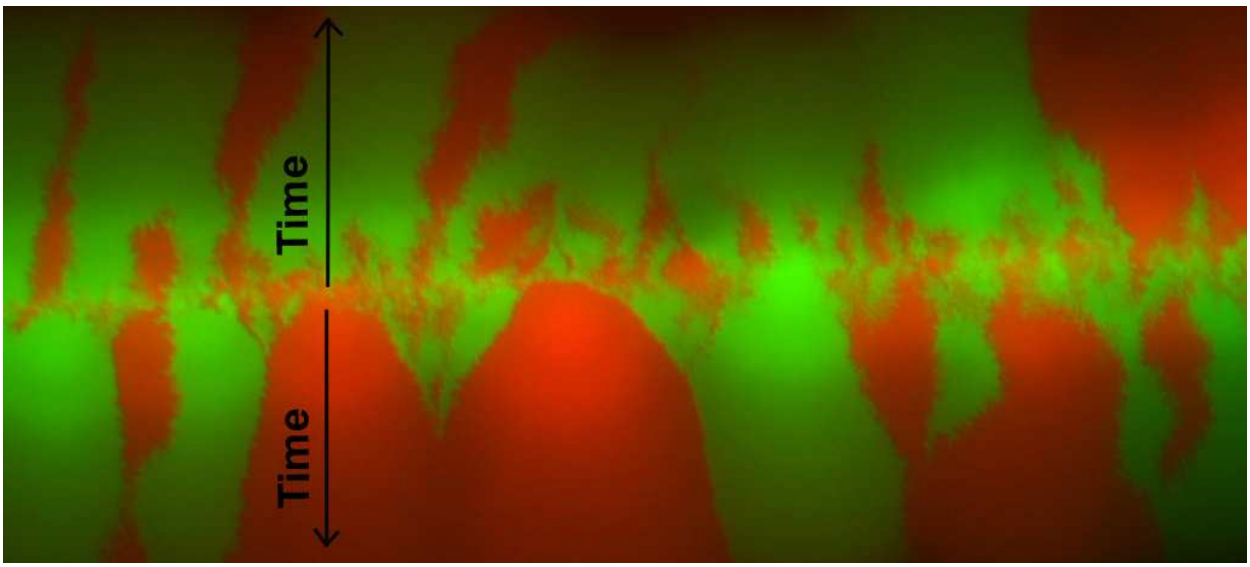

FIG. 1: (Color online) Spatial segregation in an expanding microbial population. Different colors label different alleles. Initially well-mixed population occupies a narrow horizontal linear region lying between the arrows, which show the direction of the growth. As this population expands, it segregates into well defined monoallelic domains. Details of the experiment are presented in Ref. [5].

Fisher-Kolmogorov-Petrovsky-Piscounov equation [9, 10] with additional terms representing mutation. On the other hand, when each deme contains only one organism, the model is analogous to the Eden model [11] used to describe the growth of interfaces and the voter model [12].

We also performed numerical simulations to better understand the relationship between the experiments in Ref. [5] and our analytical results. An illustrative simulation (with periodic boundary conditions) is shown in Fig. 2, which also shows the difference between a growing population front with undulations and a literally one-dimensional habitat advancing uniformly in time. Figure 3 shows qualitative agreement between the experiments and the simplified row-by-row growth model that we studied analytically.

In this paper, we first focus on the spatial segregation due to genetic drift and its effect on the dynamics of a one-dimensional population. We find that segregation of two neutral alleles has two stages. During the first stage, distinguishable domains emerge from the well-mixed population. During the second stage, domain boundaries diffuse and annihilate upon collision. As a result, some of the domains vanish whereas others grow. We show how our

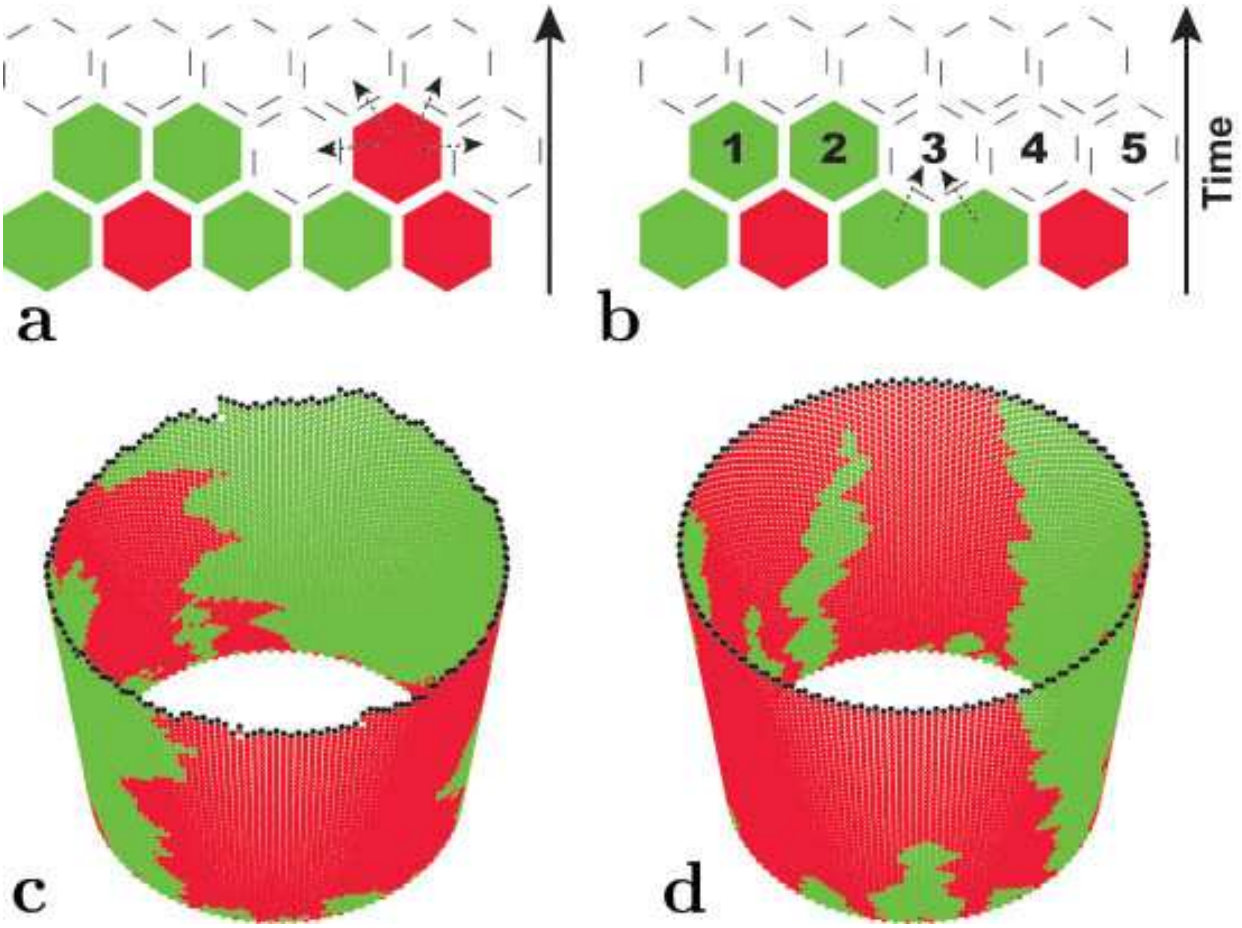

FIG. 2: (Color online) Computer simulations. The blank hexagons represent empty sites, and different colors of the occupied hexagons represent different alleles. (a) The model of an expanding population front. The highlighted hexagon is a randomly chosen cell that can reproduce and deposit an identical offspring in any of its four empty nearest neighbor sites (shown with arrows) with equal probability. (b) The model of a one-dimensional habitat. Each row represents a generation so each row is completed before moving on to the next one. An empty site can be filled only by an offspring of one of its nearest neighbors in the previous generation (shown with arrows). Both (a) and (b) show the effects of genetic drift (sampling error) when, e.g., the second from the left cell in the bottom row leaves no offspring. Such events lead to coarsening seen in (c) and (d). (c) and (d) are single simulation runs for models in (a) and (b) respectively. A population of 100 cells was wrapped around a cylinder to illustrate periodic boundary conditions used in this paper. Note that in (d) the front is flat whereas in (c) it is rough. This roughness affects some aspects of the shapes of the monoallelic domains shown in (c): A domain boundary followed from its lowest point to its highest point always goes up in (d), but, in (c), it sometimes goes down. As discussed in Ref. [5], domain walls are expected to wander more vigorously in (c) than in (d).

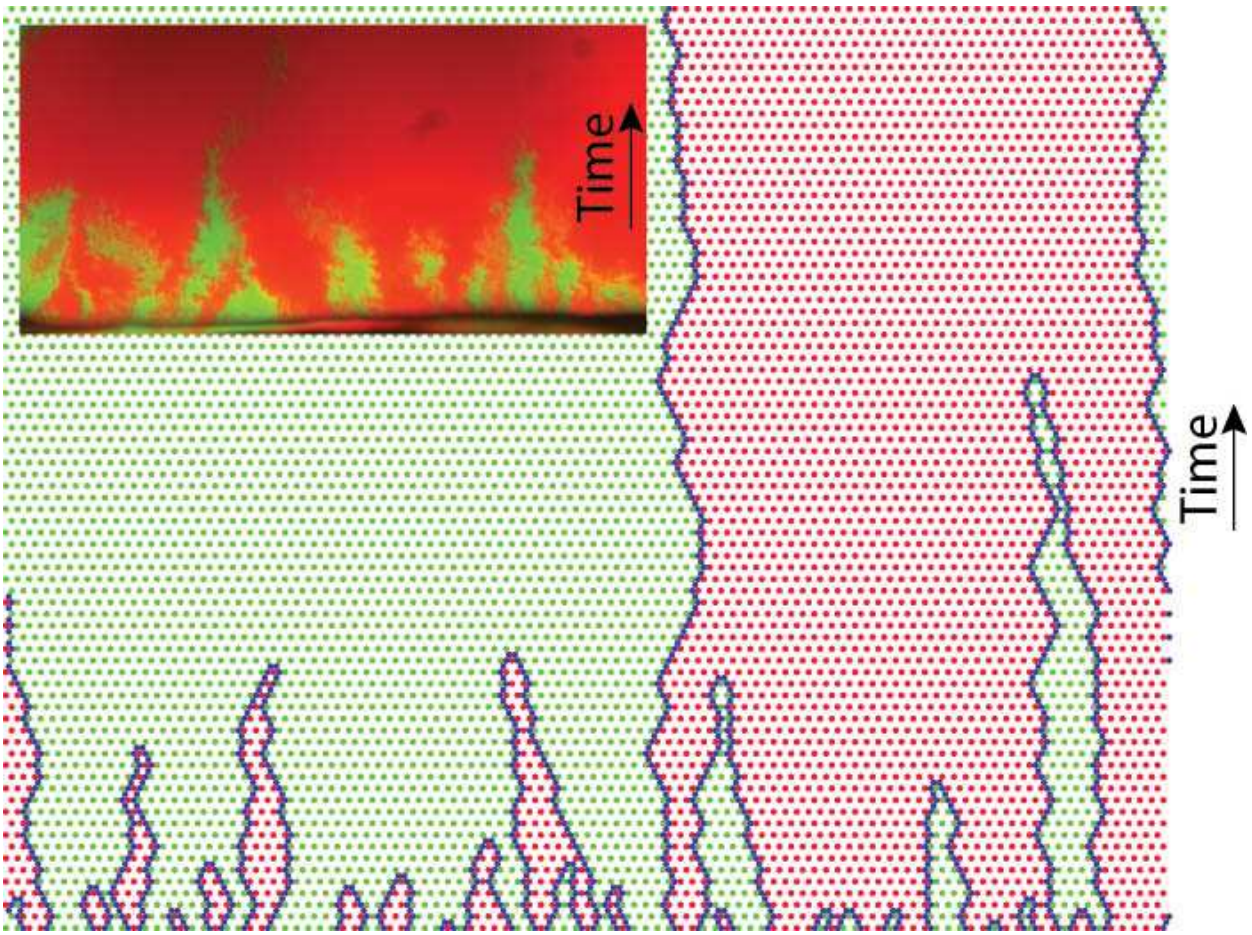

FIG. 3: (Color online) Qualitative comparison of a gene segregation experiment from a linear inoculation (inset) and the simulation of a one-dimensional habitat.

calculations might be used to extract the diffusion constant and the effective population size from experiments like those in Ref. [5], and discuss how well the model describes the behavior of microbes. A *detailed* comparison (beyond the qualitative agreement we find with the main features) would require more extensive and precise experiments; we hope such experiments will be carried out in the future. The spatial segregation dramatically changes the effects of genetic drift and selection on the population compared to the predictions of well-mixed-population models. For the neutral model without mutation, we find that local diversity or "heterozygosity" decays as $t^{-1/2}$, and the standard deviation of the global fraction of an allele grows subdiffusively as $t^{1/4}$. We also study the dynamics in the presence of weak selection and find that it differs markedly from that of a well-mixed population. Because of the spatial segregation into domains, selection acts only near domain boundaries, which

constitute only a small fraction of the population. Hence, extinction of a deleterious allele proceeds much more slowly in one-dimensional populations than in well-mixed populations. Unlike genetic drift and selection, the effects of mutation in the spatial model are essentially the same as in the well-mixed-population model, but the spatial model gives a more accurate description of the population and accounts for the spatial correlations.

A substantial fraction of our results for the neutral dynamics in a one-dimensional habitat has been derived previously in population genetics [6, 13, 14], ecology [15], and nonequilibrium statistical mechanics [12, 16]. Here, we present a single self-contained derivation of these earlier results in a novel context of expanding populations in two dimensions and in a language familiar to physicists, with future microbial tests of the theory in mind. Our new results are primarily confined to the analysis of natural selection.

This paper is organized as follows. First, we review classical results for well-mixed populations in Sec. II. We then introduce the one-dimensional stepping stone model in Sec. III and derive the equations of motion for spatial correlation functions. In Sec. IV and Sec. V we solve these equations for zero and nonzero mutation rates respectively. While the neutral stepping stone model has been treated before, we derive some new results and use a different technique that can be easily extended to radially expanding populations. The effects of selection are considered in Sec. VI, and in Sec. VII we test our analytical results with simulations. Various details are relegated to Appendices A-D. In Appendix E, we indicate how some of the 2-state (i.e., "2-allele") results can be generalized for the Potts-model-like nonequilibrium dynamics of q-alleles with $q \geq 3$.

II. POPULATION GENETICS IN WELL-MIXED POPULATIONS

Well-mixed-population models are relevant to microorganisms vigorously shaken in a test tube, but they do not describe spatial phenomena. Indeed, if cells visit all parts of the test tube during a cell division time, they are effectively zero-dimensional. Nevertheless, they can serve as a useful reference point to which spatial models can be compared. Well-mixed populations also provide a simple context to introduce genetic drift, mutation, and selection; and the stepping stone model presented in Sec. III uses a well-mixed-population model to describe the dynamics of allele frequencies within the demes. This section summarizes the classical results of nonspatial population genetics, which are primarily due to Wright, Fisher,

Haldane, and Kimura; Refs. [17] and [18] provide a good introduction to the subject and refer to the original literature, which is too extensive to be discussed here.

To simplify the discussion and to make a direct connection with the experiments in Ref. [5], we consider two alleles in a population of N haploid organisms. (For N diploid organisms, the theory is essentially the same under certain assumptions, provided one focuses on the dynamics of $2N$ gene copies in each generation; see Ref. [17].) The two-allele approximation may seem very restrictive, but many of our results can be generalized to an arbitrary integer number $q \geq 3$ of alleles. In addition, a two-allele model can be used to describe the dynamics of an allele of interest (with or without a selective advantage) when all other alleles are neutral. We assume that each of the individuals in the population can die, give birth (divide), and mutate. The details of this birth and death process are species dependent, but the dynamics on time scales larger than the generation time τ_g is believed to be universal provided N is large. This universal dynamics is often referred to as the diffusion or continuous approximation. Two simple models are commonly used to illustrate the continuous approximation: the Wright-Fisher model and the Moran model. Here, we use the latter because it more closely resembles microbes with overlapping generations.

First, we consider the Moran model without selection and mutation. During a time step, two individuals are randomly selected with replacement from the population. The first individual is chosen to reproduce, and the second one to die; thus the total number of the organisms is conserved. If the "frequency" of allele one (i.e., the fractional number of individuals with genotype one) at time step $\tilde{t}$ is $f(\tilde{t})$, then, at the next time step, it is $f + 1/N$ with probability $f(1-f)$, $f - 1/N$ with probability $f(1-f)$, and f with probability $f^2 + (1-f)^2$. The expectation value and variance of $f(\tilde{t}+1)$ are then given by,

$$\langle f(\tilde{t}+1)\rangle = f(\tilde{t}), \tag{1}$$

$$\langle [f(\tilde{t}+1) - \langle f(\tilde{t}+1)\rangle]^2\rangle = \frac{2f(\tilde{t})[1-f(\tilde{t})]}{N^2}, \tag{2}$$

where angular brackets represent average with respect to the random choice of individuals for reproduction and death. Because only one of N organisms gives birth in a Moran time step, $\tilde{t}$ measures time in fractional generation time, τ_g/N.

Equations (1) and (2) imply that $f(\tilde{t})$ performs an unbiased random walk in the space

of allele frequencies. In the continuum limit, this random walk can be described by the following Fokker-Planck equation with a frequency dependent diffusion coefficient [17, 18]

$$\frac{\partial P(t,f)}{\partial t} = \frac{\mathfrak{D}_g}{2}\frac{\partial^2}{\partial f^2}\left[f(1-f)P(t,f)\right], \tag{3}$$

where $P(t,f)$ is the probability density function for f at time t measured in generations, and $\mathfrak{D}_g$ is the genetic diffusion constant. Here, t is the time measured in generations; as discussed above, N Moran time steps constitute a generation time τ_g. Thus, in the Moran model, we have

$$\mathfrak{D}_g = \frac{1}{2N\tau_g}. \tag{4}$$

Alternative reproduction schemes, such as Wright-Fisher sampling, [17, 18] lead to an identical equation, with a different numerical coefficient in Eq. (4).

Equation (3) is subject to absorbing boundary conditions [1] at $f = 0$ and $f = 1$ because, if one of the alleles is lost, it cannot appear again in the absence of mutation. Therefore, the population eventually becomes fixed at one of the absorbing states. We calculate the rate of the fixation by considering the average heterozygosity of the population

$$H(t) \equiv \langle h(t)\rangle = \langle 2f(t)[1-f(t)]\rangle, \tag{5}$$

which is the (averaged over realizations) probability that two randomly selected individuals have different alleles. When the population is close to the fixation ($f \approx 0$ or $f \approx 1$), the heterozygosity is close to zero. The equations of motion for $F(t) \equiv \langle f(t)\rangle$ and $H(t)$ follow from Eq. (3) by multiplying both sides with f or h, integrating over f, and eliminating the derivatives with respect to f via integration by parts. The results are

$$\frac{dF(t)}{dt} = 0, \tag{6}$$

$$\frac{dH(t)}{dt} = -\mathfrak{D}_g H(t). \tag{7}$$

[1] Since Eq. 3 is singular at the boundaries, we require $\lim_{f\to\infty 0,1} f(1-f)P(t,f) = 0$. See Refs. [19] and [20] for a more detailed discussion.

Equations (6) and (7) imply that, while the average frequencies of these neutral alleles do not change $F = \langle f \rangle = f(t = 0) \equiv F_0$, the population reaches fixation exponentially fast, $H(t) = H(0)e^{-\mathfrak{D}_g t} = F_0(1 - F_0)e^{-\mathfrak{D}_g t}$.

The average heterozygosity is closely related to the variance of $f(t)$, the fraction of the first allele,

$$V(t) = \langle (f(t) - \langle f(t) \rangle)^2 \rangle = F(t)[1 - F(t)] - \frac{1}{2}H(t). \tag{8}$$

Thus, even if a population starts with zero variance, the fluctuations grow until the variance reaches its maximum value of $F_0(1 - F_0)$, which corresponds to a population fixed to allele one with probability F_0 and to allele two with probability $1 - F_0$. Note that, for small t, $V(t)$ grows linearly with time, but, at large times, the variance approaches its limiting value exponentially fast. The linear growth of variance at small times also follows from the Fokker-Planck equation because, at small times, Eq. (3) can be approximated by a diffusion equation with constant diffusivity.

Next, we generalize Eq. (3) to account for mutations. In the Moran model, mutation is included at the end of a time step by allowing the offspring to mutate with probability $\tilde{\mu}_{12}$ from allele one to allele two and with probability $\tilde{\mu}_{21}$ from allele two to allele one. If the frequency of allele one at time step $\tilde{t}$ is $f(\tilde{t})$, then, at the next time step, the expectation value of $f(\tilde{t} + 1)$ is given by

$$\langle f(\tilde{t} + 1) \rangle = f(\tilde{t}) + \frac{\tilde{\mu}_{21}[1 - f(\tilde{t})] - \tilde{\mu}_{12} f(\tilde{t})}{N}, \tag{9}$$

and the variance of $f(\tilde{t} + 1)$ is given by Eq. (2) to the leading order in the mutation rates and the inverse population size.

Since the expectation value of $f(\tilde{t})$ changes with time, mutation leads to an f-dependent drift term in the Fokker-Planck equation. Upon recalling that N Moran time steps equal one generation time, we have

$$\begin{aligned} \frac{\partial P(t,f)}{\partial t} = &- \frac{\partial}{\partial f}\left\{[\mu_{21} - (\mu_{12} + \mu_{21})f]P(t,f)\right\} \\ &+ \frac{\mathfrak{D}_g}{2}\frac{\partial^2}{\partial f^2}\left[f(1-f)P(t,f)\right], \end{aligned} \tag{10}$$

where $\mu_{12} \equiv \tilde{\mu}_{12}\tau_g^{-1}$ and $\mu_{12} \equiv \tilde{\mu}_{21}\tau_g^{-1}$ are the mutation rates per generation.

Because the alleles can mutate into each other, the probability flux through the boundaries must be zero, so Eq. (10) has reflecting boundary conditions, and a nontrivial stationary solution for $P(t, f)$ exists. While the stationary distribution can be obtained easily [18], it is sufficient to analyze the moments $F(t)$ and $H(t)$ introduced above. This will also allow us to make a direct comparison with the corresponding solutions of the one-dimensional stepping stone model in Sec. V. The equations of motion for $F(t)$ and $H(t)$ are obtained from Eq. (10) in the same way as for the absence of mutation. The results are

$$\frac{dF(t)}{dt} = \mu_{21} - (\mu_{12} + \mu_{21})F(t), \tag{11}$$

$$\frac{dH(t)}{dt} = -(\mathfrak{D}_g + 2\mu_{12} + 2\mu_{21})H(t) + 2[\mu_{21} + (\mu_{12} - \mu_{21})F(t)]. \tag{12}$$

Since these equations are linear differential equations with constant coefficients, the equilibrium is approached exponentially fast. The stationary solutions, which are obtained in the limit $t \to \infty$, are given below

$$F(\infty) = \frac{\mu_{21}}{\mu_{12} + \mu_{21}}, \tag{13}$$

$$H(\infty) = \frac{2F(\infty)[1 - F(\infty)]}{1 + \frac{\mathfrak{D}_g}{2(\mu_{12}+\mu_{21})}}. \tag{14}$$

From Eqs. (14) and (8), we see that, when the population size is large enough, i.e. $\mathfrak{D}_g \ll (\mu_{12} + \mu_{21})$, $H(\infty) \approx 2F(\infty)[1 - F(\infty)]$, the stationary value of the heterozygosity is consistent with $f(t) \approx F(\infty)$. Thus $V(\infty) \approx 0$, and the fluctuations of $f(t)$ are negligible. In the opposite limit, $H(\infty) \propto \frac{\mu_{12}+\mu_{21}}{\mathfrak{D}_g}$ is significantly smaller, which suggests that most of the time the population is fixed to one of the alleles, and mutations lead to rare transitions between states with $f = 0$ and $f = 1$. Our interpretation of Eq. (14) is consistent with a more rigorous analytical and numerical analysis by Duty [21].

Finally, we introduce Darwinian natural selection, which is usually related to the difference in the reproduction or survival probability of the organisms. In the continuous time limit considered here, both mechanisms of selection lead to the same dynamics; therefore, we only consider selection due to different growth rates. In the Moran model, a growth rate difference is embodied in modified probabilities of reproduction: the individual with

allele one is chosen to reproduce not with probability f but with probability $\frac{w_1 f}{w_1 f + w_2(1-f)}$, where w_1 and w_2 are the fitnesses (i.e., growth rates) of alleles one and two respectively. In the absence of mutations, this modification results in

$$\langle f(\tilde{t}+1)\rangle = f(\tilde{t}) + \frac{f(\tilde{t})[1-f(\tilde{t})](w_1 - w_2)}{N\{w_1 f(\tilde{t}) + w_2[1-f(\tilde{t})]\}}. \tag{15}$$

When selection is weak, that is $|w_1 - w_2| \ll w_1 + w_2$, Eq. (15) reduces to

$$\langle f(\tilde{t}+1)\rangle = f(\tilde{t}) + \frac{\tilde{s}}{N} f(\tilde{t})[1-f(\tilde{t})], \tag{16}$$

where $\tilde{s} = 2(w_1 - w_2)/(w_1 + w_2)$ is the selective advantage of allele one, which has to be much smaller than one for the approximation to hold. When $\tilde{s} > 0$, allele one is advantageous; for $\tilde{s} < 0$, it is deleterious. In the following, we assume that allele one is advantageous because one can always relabel the alleles to satisfy this condition.

Similar to the case of mutations without selection, the variance of $f(\tilde{t}+1)$ is given by Eq. (2) to the leading order in $\tilde{s}$ and N^{-1}, and the Fokker-Planck equation at the level of the generation time τ_g acquires an f-dependent drift term due to selection:

$$\begin{aligned} \frac{\partial P(t,f)}{\partial t} = & -s\frac{\partial}{\partial f}\left[f(1-f)P(t,f)\right] \\ & + \frac{\mathfrak{D}_g}{2}\frac{\partial^2}{\partial f^2}\left[f(1-f)P(t,f)\right], \end{aligned} \tag{17}$$

where $s = \tilde{s}\tau_g^{-1}$. The equations for F and H are not as useful as before because the hierarchy of the moment equations does not close. Nevertheless, Eq. (17) can be easily analyzed in two limits. When the population size is large ($\mathfrak{D}_g \ll s$), fluctuations are not important, and $\frac{dF(t)}{dt} \approx sF(t)[1-F(t)]$. Upon setting $F_0 \equiv F(0)$, we have

$$F(t) \approx \frac{1}{1 + \frac{1-F_0}{F_0} e^{-st}}, \tag{18}$$

so the selective sweep is exponentially fast. When the fluctuations dominate the dynamics, the selection slightly increases the odds of fixation of the advantageous allele, but does not significantly affect the rate of fixation. For a detailed analysis of Eq. (17) see Ref. [18].

In the continuous limit, the population genetics of a well-mixed effectively zero-dimensional population with genetic drift, selection, and mutation is summarized by the following Fokker-Planck (or forward Kolmogorov) equation:

$$\begin{aligned}\frac{\partial P(t,f)}{\partial t} =& -s\frac{\partial}{\partial f}\left[f(1-f)P(t,f)\right] \\ & -\frac{\partial}{\partial f}\left\{[\mu_{21}-(\mu_{12}+\mu_{21})f]P(t,f)\right\} \\ & +\frac{\mathfrak{D}_g}{2}\frac{\partial^2}{\partial f^2}\left[f(1-f)P(t,f)\right].\end{aligned} \tag{19}$$

Although this formulation is appropriate for nonspatial models, an alternative formulation via a stochastic differential equation can be generalized to the spatial models more easily. Equation (19) is equivalent to

$$\frac{df(t)}{dt} = sf(t)[1-f(t)] + \mu_{21} - (\mu_{12}+\mu_{21})f(t) + \sqrt{\mathfrak{D}_g f(t)[1-f(t)]}\Gamma(t) \quad (It\hat{o}), \tag{20}$$

$$\langle \Gamma(t_1)\Gamma(t_2)\rangle = \delta(t_1-t_2), \tag{21}$$

where $\Gamma(t)$ is a white, zero mean Gaussian noise, and $\delta(t)$ is Dirac's delta-function; to get the correct Fokker-Planck Equation (19), one must use Itô's prescription to define how Eq. (20) steps the dynamics forward in time. This interpretation of the noise term ensures that $f(t)$ depends only on $\Gamma(t')$ with $t' < t$ as it is appropriate for population genetics. Itô's prescription is adopted throughout the paper, and a brief introduction to the Itô calculus is given in Appendix D (see also Refs. [19, 21, 22]). In Sec. III, we use Eq. (20) to formulate the stepping stone model in one dimension.

Well-mixed-population-models do not describe migration and subdivision of natural populations [17]. To remedy this deficiency, two common approaches exist: to assume a uniformly populated spatial habitat with free diffusion or to assume a patchy habitat with a prescribed pattern of limited migration between the patches. The former is the subject of this paper, and can be regarded as the continuum limit of the stepping stone model [6], see Sec. III. The simplest variant of the latter approach is known as the island model [23]. The island model assumes that all patches or islands have the same number of organisms and populations in every patch obey well-mixed-population dynamics. The migration occurs between *any* two patches with equal probability, so, in some sense, this is a mean field or infinite-dimensional model. The island model successfully predicts that the organisms are more likely to be related locally than globally, but most of its predictions are similar to

those of well-mixed-population models because the migration does not account for spatial structure. In the limit of an infinitely large number of islands, the effect of migration in and out of any patch is equivalent to an effective mutation rate; however, this is not the case in a one-dimensional model considered below.

III. ONE-DIMENSIONAL STEPPING STONE MODEL

In Sec. II, we formulated a model to describe genetic drift, mutation, and selection in an effectively zero-dimensional habitat. For a one-dimensional population considered in this section, we extend the model to account for short range migrations during every generation. Migration is usually modeled either as exchange of individuals between neighboring island populations (demes) [6, 23] or as dispersal of offspring or adults within a continuous population [7, 13, 24]. Although the first approach was developed to model patchy populations, it can be used to describe continuous populations if the deme sizes are much smaller than the whole population, and spatial variations are gradual. In this limit, both migration models should give essentially the same results. Here, we start with first approach because it is conceptually simpler.

To specify the one-dimensional stepping stone model, we consider an infinite set of demes arranged on a line. Neighboring demes are separated by distance a and indexed by an integer $l = -\infty, ..., -1, 0, 1, ..., \infty$. Each deme has N organisms (but the total population size is infinite), and the frequency of allele one in deme l is $f_l(t)$. Migration occurs only between nearest neighbors, and, every generation, a deme exchanges $\tilde{m}N$ individuals with its right neighbor and $\tilde{m}N$ individuals with its left neighbor. We assume that the exchange fraction $\tilde{m}$ is much smaller than one, and that the individuals of both allelic types are equally likely to be exchanged. Thus, in one generation, $\langle f_l \rangle$ changes by $\tilde{m}(f_{l-1} + f_{l+1} - 2f_l)$ due to migration. The variance of f_l grows due to randomness in the exchange process, but this increase is negligible compared to the genetic drift within an island. In the continuous time limit, $f_l(t)$ obeys the following generalization of Eq. (20):

$$\frac{df_l}{dt} = m(f_{l-1} + f_{l+1} - 2f_l) + sf_l(1-f_l) + \mu_{21} - (\mu_{12} + \mu_{21})f_l + \sqrt{\mathfrak{D}_g f_l(1-f_l)}\Gamma_l \quad (It\hat{o}), \quad (22)$$

$$\langle \Gamma_{l_1}(t_1)\Gamma_{l_2}(t_2)\rangle = \delta_{l_1 l_2}\delta(t_1 - t_2), \tag{23}$$

where $m = \tilde{m}\tau_g^{-1}$ and $\delta_{l_1 l_2}$ is Kronecker's delta. We can also write Eq. (22) in the continuous space limit by introducing a spatial coordinate $x = la$,

$$\frac{\partial f}{\partial t} = D_s \frac{\partial^2 f}{\partial x^2} + sf(1-f) + \mu_{21} - (\mu_{12} + \mu_{21})f + \sqrt{D_g f(1-f)}\Gamma \quad (It\hat{o}), \tag{24}$$

$$\langle \Gamma(t_1, x_1)\Gamma(t_2, x_2)\rangle = \delta(t_1 - t_2)\delta(x_1 - x_2), \tag{25}$$

where the spatial and genetic diffusion constants are $D_s = ma^2$ and $D_g = a\mathfrak{D}_g = \frac{a}{2\tau_g N}$ respectively. Thus, the continuous time and space limit the stepping stone model is described by the stochastic Fisher-Kolmogorov-Petrovsky-Piscounov equation [9, 10] with additional terms describing mutation.

Similar to the analysis of the well-mixed-population model discussed in Sec. II, we use equal-time correlation functions of $f(t, x)$ to characterize the dynamics of the stepping stone model. The spatial versions of the average frequency and heterozygosity are defined as follows:

$$F(t, x) = \langle f(t, x)\rangle, \tag{26}$$

$$H(t, x_1, x_2) = \langle f(t, x_1)[1 - f(t, x_2)]\rangle + \langle f(t, x_2)[1 - f(t, x_1)]\rangle. \tag{27}$$

The equation of motion for $F(t, x)$ depends on $H(t, x, x)$, and is readily derived by averaging Eq. (24), which gives

$$\frac{\partial F}{\partial t} = D_s \frac{\partial^2 F}{\partial x^2} + \mu_{21} - (\mu_{12} + \mu_{21})F + \frac{s}{2}H(t, x, x). \tag{28}$$

The dynamics of $H(t, x_1, x_2)$ is obtained by using Itô's formula (see Appendix D) to differentiate Eq. (27) with respect to t and then eliminating $\frac{\partial f}{\partial t}$ with the help of Eq. (24). The result is

$$\frac{\partial}{\partial t}H(t,x_1,x_2) = D_s\left(\frac{\partial^2}{\partial x_1^2}+\frac{\partial^2}{\partial x_2^2}\right)H(t,x_1,x_2) - D_g H(t,x_1,x_2)\delta(x_1-x_2) - 2(\mu_{12}+\mu_{21})H(t,x_1,x_2)+$$
$$2\mu_{21} + (\mu_{12}-\mu_{21})[F(t,x_1)+F(t,x_2)] + \frac{s}{2}[H(t,x_1,x_1)+H(t,x_2,x_2)]-$$
$$s\langle 2f(t,x_1)[1-f(t,x_1)]f(t,x_2)\rangle - s\langle 2f(t,x_2)[1-f(t,x_2)]f(t,x_1)\rangle. \tag{29}$$

Equations (28) and (29) agree with the ones derived in Ref. [25] in the limit of no mutations considered there.

From Eq. (29), one can see that the hierarchy of the moment equations does not close unless selection is absent. Similar to the well-mixed case, the correlation functions for neutral models with and without mutations can be found analytically, see Secs. V and IV, but different methods are required to analyze the dynamics in the presence of selection, see Sec. VI. To simplify the analysis, we consider well-mixed, spatially homogeneous initial conditions. Then F is only a function of t, and H is a function of t and $x = x_1 - x_2$. With these simplifying assumptions, the equations of motion for $F(t)$ and $H(t,x)$ take the following form:

$$\frac{dF(t)}{dt} = \mu_{21} - (\mu_{12}+\mu_{21})F(t) + \frac{s}{2}H(t,0), \tag{30}$$

$$\frac{\partial}{\partial t}H(t,x) = 2D_s\frac{\partial^2}{\partial x^2}H(t,x) - D_g H(t,0)\delta(x) - 2(\mu_{12}+\mu_{21})H(t,x)+$$
$$2\mu_{21} + 2(\mu_{12}-\mu_{21})F(t,x) + sH(t,0) - 2s\langle 2f(t,x_1)[1-f(t,x_1)]f(t,x_2)\rangle. \tag{31}$$

IV. NEUTRAL MODEL WITHOUT MUTATION

We start the analysis of the one-dimensional stepping stone model by considering neutral alleles that do not mutate. In practice, this means $N^2\tilde{\mu}_{12}, N^2\tilde{\mu}_{21} \ll 1$ and $N^2\tilde{s} \ll 1$ (as we show below). Although these assumptions are not always realistic, they help to clarify the role of genetic drift in a spatial context. In addition, neglecting mutations is a good approximation on time scales shorter than the waiting times for the mutations μ_{12}^{-1} and μ_{21}^{-1}. Under these assumptions, F does not change, $F(t) = F_0$, and Eq. (31) reads

$$\frac{\partial}{\partial t}H(t,x) = 2D_s\frac{\partial^2}{\partial x^2}H(t,x) - D_g H(t,0)\delta(x). \tag{32}$$

Equation (32) can also be derived by tracing the lineages of organisms backward in time. The spatial heterozygosity, $H(t,x)$, is the average probability of sampling two different individuals chosen at time t from demes separated by distance x. As we trace the lineages of the two sampled organisms backward in time, the lineages diffuse in space due to migration and when they are at the same point they have a chance to coalesce, in which case the sampled organisms must be identical because they have a common ancestor. Such a coalescence event changes the probability of being different from H to 0, and acts like a sink at $x = 0$. The first term on the right hand side of Eq. (32) describes the diffusion, and the second term describes the coalescence. Since this argument is valid for an arbitrary number of alleles, Eq. (32) is valid for an arbitrary number of spatially diffusing neutral alleles. See Appendix E for a more detailed discussion of the q-allele problem, with $q \geq 3$.

To better understand the microbiology experiments on neutral alleles by Hallatschek *et al.* [5], we consider uncorrelated initial conditions $F(0) = F_0$ and $H(0,x) = H_0$, where F_0 is the fraction of allele one and $H_0 = 2F_0(1-F_0)$, which is the heterozygosity of a well-mixed population with the frequency of allele one equal to F_0. For these initial conditions, Eq. (32) is solved in Appendix A. The results are

$$H(t,x) = H_0 - H_0 D_g \int_0^t dt' \frac{e^{-\frac{x^2}{8D_s(t-t')}}}{\sqrt{8\pi D_s(t-t')}} \operatorname{erfc}\left(\sqrt{\frac{D_g^2 t'}{8D_s}}\right) e^{\frac{D_g^2 t'}{8D_s}}, \tag{33}$$

$$H(t,0) = H_0 \operatorname{erfc}\left(\sqrt{\frac{D_g^2 t}{8D_s}}\right) e^{\frac{D_g^2 t}{8D_s}}, \tag{34}$$

where $\operatorname{erfc}(y)$ is the complementary error function.

The spatial heterozygosity at vanishing separation, $H(t,0)$, is particularly interesting because it indicates the degree of spatial segregation: if $H(t,0) \ll 1$, then, locally, the demes are fixed to one of the two alleles. From Eq. (34), one can see that, for $t \gg 8D_s/D_g^2$,

$$H(t,0) = H_0\left(\frac{\pi D_g^2 t}{8D_s}\right)^{-1/2} + O(t^{-3/2}), \tag{35}$$

which means that at long times one of the alleles reaches fixation locally. Therefore, we see that the spatial model we are considering is consistent with the experiments by Hal-

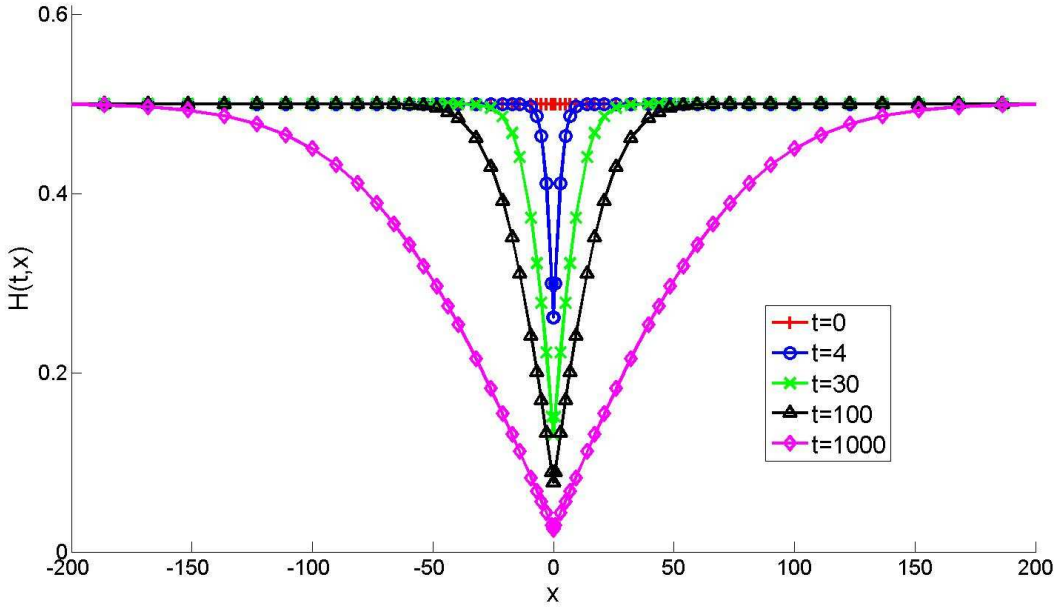

FIG. 4: (Color online) Solutions of Eq. (32) at various times, given $H(0,x) = \frac{1}{2}$. Time and distance are measured in untis such that $D_s = 1$ and $D_g = 1$. Time increases from the top curves to the bottom curves. Note the statistical reflection symmetry, $H(t,x) = H(t,-x)$

latschek *et al.* [5] (see Fig. 1) because it predicts the formation of domains (the regions of local fixation). Thus, similar to the well-mixed model considered in Sec. II, one of the alleles reaches fixation locally with fixation time $\tau_f = 8D_s/(\pi D_g^2) \sim N^2$. But not only is this fixation time proportional to N^2, instead of N, the functional form of heterozygosity decay different: instead of a rapid exponential decay, the spatial model shows a slow algebraic decay of local heterozygosity. These results agree with the previous works on population genetics by Malécot [13] and Nagylaki [24]. Local fixation and $t^{-1/2}$ decay of local heterozygosity have also been found in the voter model [12], which corresponds to the stepping stone model with $N = 1$.

The characteristic demixing time can also be estimated by the following scaling argument: the *effective* population size at time t in the coarsening process is $N_{eff}(t) \sim n_0\sqrt{tD_s}$, where the population density $n_0 \sim N/a$. Upon recalling that the fixation time in zero dimensions is $\tau_f = N_{eff}\tau_g$, and solving self-consistently for τ_f, we have $\tau_f \sim D_s N^2 \tau_g^2/a^2 \sim D_s/D_g^2 \sim N^2\tau_g$.

Another important characteristic of $H(t,x)$ is the length scale over which $H(t,x)$ changes

from its minimum to its maximum values. Figure 4 plots Eq. (33) and shows the spatial variation of $H(t,x)$ at different times. One can see that the spatial heterozygosity is reduced near the origin due to the local fixation, but $H(t,x)$ rises to its initial value H_0 at large x, where the alleles remain uncorrelated. After the domains form, i.e. for $t \gg 8D_s/D_g^2$, this change from $H(t,0)$ to $H(0,x)$ happens on a length scale that is set by the average size of the domains ℓ, which is proportional to the diffusion length $\sqrt{2D_s t}$, as follows from Eq. (33). Since this characteristic length scale changes with time, it is convenient to rescale distances: $\bar{x} = x/\sqrt{2D_s t}$. Upon using Eq. (35) to simplify Eq. (33), we see that $H(t,x)$ approaches a nontrivial limit in terms of $\bar{x}$ as time goes to infinity:

$$H(t,\bar{x}) \stackrel{t\to\infty}{\longrightarrow} H_0 \left(1 - \frac{1}{\pi} \int_0^1 \frac{d\zeta}{\sqrt{\zeta(1-\zeta)}} e^{-\frac{|\bar{x}|^2}{4\zeta}} \right), \tag{36}$$

which agrees with the known results for the voter model [12].

A more precise evaluation of the domain density and hence an average domain size $\ell(t)$ can be obtained by differentiating $H(t,x)$, as shown in Appendix B. From Eq. (B4), we know that $\ell(t) = \frac{4D_s}{D_g H(t,0)}$, so using Eq. (35) we see that

$$\ell = \frac{\sqrt{2\pi D_s t}}{2f_0(1-f_0)}, \tag{37}$$

which is consistent with the analysis of Ref. [26]. Note that the genetic diffusion constant $D_g \sim 1/N$ drops out. As discussed in Ref. [26], at large times the only dynamics left is the motion of the domain boundaries; with neutral alleles, these walls behave as annihilating random walks, and the average domain size can be easily calculated.

Equations (34) and (37) suggest that the processes driven by the genetic drift slow down with time because the logarithmic time derivatives of $H(t,0)$ and ℓ tend to zero as time goes to infinity. In the annihilating random walk picture of Ref. [26], annihilations become rarer and rarer as the coarsening progresses. A more direct measure of genetic drift, which is also interesting from the biological point of view, is the fluctuations of the total fraction of, say, the first allele $\mathfrak{f}(t)$ in a finite population of length L. We define $\mathfrak{f}(t)$ as

$$\mathfrak{f}(t) = \frac{1}{L} \int_0^L f(t,x) dx, \tag{38}$$

and compute its variance $\nu(t)$ to characterize its fluctuations.

Upon integrating Eq. (24)over x with $s = \mu_{12} = \mu_{21} = 0$, we obtain the equation of motion for $\mathfrak{f}$:

$$\frac{d\mathfrak{f}}{dt} = \frac{1}{L}\int_0^L \sqrt{D_g f(t,x)[1-f(t,x)]}\Gamma(t,x)dx, \tag{39}$$

where the spatial diffusion term vanishes after integration by parts provided periodic or Newman boundary conditions are imposed. Upon noting that $\langle\mathfrak{f}\rangle = F = \text{const}$ (the Itô interpretation of the noise $\Gamma(t,x)$ is crucial here) and defining

$$\nu = \langle\mathfrak{f}^2\rangle - \langle\mathfrak{f}\rangle^2, \tag{40}$$

one finds immediately that $\frac{d\nu}{dt} = \frac{d}{dt}\langle\mathfrak{f}^2\rangle$. To evaluate the time derivative, we use the rules of the Itô calculus, sketched in Appendix D, and find

$$\frac{d\nu(t)}{dt} = \frac{1}{L^2}\int_0^L\int_0^L \sqrt{D_g f(t,x_1)[1-f(t,x_1)]}\sqrt{D_g f(t,x_2)[1-f(t,x_2)]}\delta(x_1-x_2)dx_1dx_2, \tag{41}$$

where the delta function comes from averaging over the noise and using Eq. (25). From Eq. 41, it follows that

$$\nu(t) = \frac{D_g}{2L}\int_0^t H(t',0)dt', \tag{42}$$

where we assume $\nu(0) = 0$. Hence, we know $\nu(t)$ exactly because $H(t,0)$ is given by Eq. (34).

For small times, $t \ll 8D_s/D_g^2$, the variance grows linearly with time. For large times, we can use the asymptotic expansion of $H(t,0)$ given by Eq. (35) to calculate $\nu(t)$. The result is

$$\nu(t) = \frac{H_0\sqrt{8D_s t}}{\sqrt{\pi}L} + O\left(\frac{D_s}{D_g L}\right). \tag{43}$$

Equation (43) is consistent with Ref. [16], and we immediately conclude that the standard deviation $\Delta(t) = \sqrt{\nu(t)}$ grows as $t^{1/4}$ for large times! This important result for q-alleles is re-derived in Appendix E by approximating the dynamics of the domain boundaries by annihilating random walks. Thus, $\mathfrak{f}$ performs a subdiffusive random walk, and the action of genetic drift on the global frequency $\mathfrak{f}(t)$ becomes weaker with time. Equation (43) is valid only for $t \ll \frac{L^2}{D_s}$ because it relies on Eq. (35), which is valid for an infinite population, and

should break down at times that are long enough for a domain boundary to diffuse from one end of the population to the other. Using Equations (8) and (42), one can also calculate the behavior of the global heterozygosity $\mathcal{H}(t) = L^{-1}\int_0^L H(t,x)dx$, i.e. the probability to sample two different alleles from the population regardless of their spatial locations:

$$2F_0(1-F_0) - \mathcal{H}(t) = \frac{D_g}{L}\int_0^t H(t',0)dt' = \frac{H_0\sqrt{32D_s t}}{\sqrt{\pi}L} + O\left(\frac{D_s}{D_g L}\right), \tag{44}$$

where the second equality requires $t \ll \frac{L^2}{D_s}$ for the reasons mentioned above. In the opposite limit $t \gg \frac{L^2}{D_s}$, the global heterozygosity $\mathcal{H}(t,x)$ obeys zero-dimensional dynamics of a well-mixed population with an effective population size $L/(2D_g)$ as shown in Ref. [24].

The local heterozygosity and average domain size can be obtained from experiments on microbial spreading like the one shown in Fig. 1. If the data are sufficiently precise, Eqs. (35) and (37) could be used to extract D_s and D_g from the experiments. Since $D_g \sim 1/N$, extracting D_g from experimental data determines the effective deme size for the equivalent stepping stone model. D_s can be obtained from the diffusion of individual domain boundaries or $\nu(t)$. These two parameters completely determine the neutral dynamics without mutation and play an important role when selection or mutation is present.

V. NEUTRAL MODEL WITH MUTATION

While on short time scales mutation can be neglected, it is the long time scales and the patterns of genetic diversity created by mutations that are of particular interest in population genetics. Noticeable mutations also arise in microbiology experiments like those in Fig. 1, especially if mutation rates are enhanced by DNA damaging chemicals or radiation. In this section, we extend the results of Sec. IV by allowing for nonzero mutation rates between the two alleles. We assume as before statistically homogeneous initial conditions, and note that the dynamics of the dynamics of the one and two-point correlation functions is then given by

$$\frac{dF(t)}{dt} = \mu_{21} - (\mu_{12} + \mu_{21})F(t), \tag{45}$$

$$\frac{\partial}{\partial t}H(t,x) = 2D_s\frac{\partial^2}{\partial x^2}H(t,x) - D_g H(t,x)\delta(x) - 2(\mu_{12}+\mu_{21})H(t,x) + 2\mu_{21} + 2(\mu_{12}-\mu_{21})F(t), \tag{46}$$

where $F(t) \equiv \langle f(t,x)\rangle$ is independent of x. The equation of motion for F in the spatial model is exactly the same as Eq. (11), which describes the well-mixed-population model. Therefore, F relaxes to its equilibrium value, $F(\infty) = \frac{\mu_{21}}{\mu_{12}+\mu_{21}}$, [see Eq. (13)] exponentially fast with time constant $(\mu_{12}+\mu_{21})^{-1} \gg \tau_g$. The similarity to the nonspatial model is not surprising because neutral mutations occur equally likely at any point within the population, regardless of its spatial structure. The dynamics of $H(t,x)$ is, however, more complicated because both mutation and genetic drift determine the behavior of the spatial heterozygosity.

The stationary solution of Eq. (46) reads

$$H(\infty,x) = \frac{2\mu_{12}\mu_{21}}{(\mu_{12}+\mu_{21})^2}\left(1 - \frac{e^{-\sqrt{\frac{\mu_{12}+\mu_{21}}{D_s}}|x|}}{1+4\sqrt{\frac{D_s(\mu_{12}+\mu_{21})}{D_g^2}}}\right). \tag{47}$$

Equation (47) agrees with the solution by Kimura and Weiss [6], which was obtained in the discrete space and time limit. One can see that, for $x \gg \sqrt{\frac{D_s}{\mu_{12}+\mu_{21}}}$, the spatial heterozygosity approaches $2F(\infty)[1-F(\infty)]$. Thus, mutations cause the frequencies of allele one to eventually become uncorrelated at large separations. At shorter distances, however, there are correlations, and $H(\infty,x) < H(\infty,\infty)$ for all $x < \infty$. Note, in particular, that

$$H(\infty,0) = \frac{2F(\infty)[1-F(\infty)]}{1+\frac{1}{4}\sqrt{\frac{D_g^2}{D_s(\mu_{12}+\mu_{21})}}} < H(\infty,\infty). \tag{48}$$

Note also that, for small mutation rates, the heterozygosity is proportional to $\mu_{12}+\mu_{21}$ [see Eq. (14)] in a well-mixed population, but the local heterozygosity in a one-dimensional population is proportional to $\sqrt{\mu_{12}+\mu_{21}}$ whenever $\tau_g(\mu_{12}+\mu_{21}) \ll a^2/(N^2 D_s \tau_g)$, which is a consequence of weaker genetic drift in one dimension [2].

When $H(\infty,0) \ll H(\infty,\infty)$, the population is segregated into domains of different allelic types. Upon invoking Eq. (B4) we obtain the following average domain size:

[2] In population genetics, population structure and spatial correlations are often reported via $F_{\rm st} = H(\infty,0)/H(\infty,\infty)$, which can readily be obtained from Eq. (48).

$$\ell = \frac{2D_s(\mu_{12}+\mu_{21})^2}{D_g\mu_{12}\mu_{21}}\left(1+\frac{1}{4}\sqrt{\frac{D_g^2}{D_s(\mu_{12}+\mu_{21})}}\right) \approx \frac{D_s^{\frac{1}{2}}(\mu_{12}+\mu_{21})^{\frac{3}{2}}}{2\mu_{12}\mu_{21}}, \tag{49}$$

in the limit discussed above. This result, together with Eq. (13), can be used to extract the mutation rates from experimental data.

We can also determine how fast $H(t,x)$ reaches its stationary value. Since the heterozygosity cannot be in equilibrium unless the frequency of the alleles has equilibrated, we assume for simplicity that $F(0)$ equals its stationary value. Then, the deviation of the spatial heterozygosity from its long time equilibrium value $\tilde{H}(t,x) = H(t,x) - H(\infty,x)$ obeys the following equation:

$$\frac{\partial}{\partial t}\tilde{H} = 2D_s\frac{\partial^2}{\partial x^2}\tilde{H} - D_g\tilde{H}\delta(x) - 2(\mu_{12}+\mu_{21})\tilde{H}. \tag{50}$$

Equation (50) can be further simplified by the change of variables $\tilde{H} = e^{-2(\mu_{12}+\mu_{21})t}\hat{H}$, which leads to

$$\frac{\partial}{\partial t}\hat{H} = 2D_s\frac{\partial^2}{\partial x^2}\hat{H} - D_g\hat{H}\delta(x). \tag{51}$$

Since Eq. (51) is identical to Eq. (32), we conclude that, at long times, the difference between $H(t,x)$ and the stationary solution decays as $C\sqrt{\frac{D_s}{D_g^2 t}}e^{-2(\mu_{12}+\mu_{21})t}$, where C is a constant. Thus, apart from an algebraic prefactor (and a nontrivial spatial dependence), the dynamics of $H(t,x)$ is essentially the same as in the well-mixed case.

In this section, we considered a model with only two alleles; however, in many circumstances, an infinite alleles model is more appropriate. The infinite alleles model is briefly discussed in Appendix C. Some results for$q$-alleles, $2 < q < \infty$, are discussed in Appendix E.

VI. SELECTION

Unlike the neutral models with spatial diffusion and mutation discussed above, the one-dimensional stepping stone model with selection cannot be treated analytically because the hierarchy of moment equations does not close. We briefly examined three closure schemes:

$$\langle 2f(t,x_1)[1-f(t,x_1)]f(t,x_2)\rangle \approx H(t,0)F(t), \tag{52}$$

$$\langle 2f(t,x_1)[1-f(t,x_1)]f(t,x_2)\rangle \approx 2F(t)[1-F(t)][1-2F(t)]-[1-2F(t)]H(t,x)+H(t,0)F(t), \tag{53}$$

and

$$\langle f(t,x_1)f(t,x_2)f(t,x_3)\rangle \approx \frac{\langle f(t,x_1)f(t,x_2)\rangle\langle f(t,x_2)f(t,x_3)\rangle}{F}, \quad \text{assuming} \quad x_1 \le x_2 \le x_3. \tag{54}$$

The first scheme is a simple factorization approximation; the second scheme, which assumes small fluctuations, is due to Nagylaki [25]; and the third scheme, which provides a good approximation for some diffusion limited reactions, was proposed in Ref. [27]. Unfortunately, none of the schemes describe the behavior of the system correctly. The progress can be made, however, for some initial conditions in two limiting cases of strong selection $\frac{sD_s}{D_g^2} \gg 1$ and weak selection $\frac{sD_s}{D_g^2} \ll 1$. For the rest of this section, we include spatial diffusion and genetic drift, but neglect mutations, which is justified on short time scales.

First, let us consider the initial condition $f(0,x) = 1-\theta(x)$, where $\theta(x)$ is the Heaviside step function. This initial condition specifies just one domain boundary, which, for any positive s, undergoes Brownian motion with a drift to the right. This is a good description of an expansion of a new advantageous mutant spreading through the population. In the strong selection limit ($s \gg D_g^2/D_s$), R. A. Fisher [9] found that the sharp boundary above broadens to a width of order $\sqrt{D_s/s}$, and the velocity of the genetic wave is given by

$$v_s = 2\sqrt{sD_s}. \tag{55}$$

When, in contrast, selection is weak compared to genetic drift, Doering, Mueller, and Smereka [28] recently found that the velocity is given by,

$$v_w = \frac{2sD_s}{D_g}. \tag{56}$$

When the population contains multiple domains, the domain walls bordering a favorable genetic variant ("allele one") expand to engulf the regions occupied by the more deleterious allele.

Another interesting initial condition is $f(0,x) = F_0 = \text{const.}$, i.e. the population is initially well-mixed. This scenario, for example, describes the quasi-one-dimensional strip of

pioneers advancing at the front of a two-dimensional population wave that originated from a well-mixed ancestral population and is propagating in the region where one of the alleles has higher fitness (see Ref. [26]). If selection is strong enough, then allele one ("the preferred variant") takes over the population before spatial correlations have time to appear. To see this, note from Eq. (18) that allele one wins locally on the time scales of s^{-1}, but, from Eq. (34), the time for spatial correlations to appear is on the order of D_s/D_g^2, which is much larger than s^{-1} in the strong selection limit. Thus, the behaviors of one-dimensional and well-mixed populations are similar when $s \gg D_g^2/D_s = a^2/(\tau_g^2 N^2 D_s)$.

In the limit of weak selection, however, spatial correlations appear before allele two is eliminated, which changes the dynamics of the system. Qualitatively, we can divide the selective sweep into two stages. During the first stage, the effects of selection are negligible and spatial segregation occurs as described in Sec. IV. During the second stage, the domains of allele two shrink at each end with wall velocity v_w given by Eq. (56), and the stochastic motion of the domain boundaries can be neglected. The crossover time between the stages occurs when the diffusive displacement of the walls is of the same order as their deterministic displacement, that is when $v_w t = \sqrt{2D_s t}$. Thus, the crossover time τ^* is on the order of D_s/v_w^2, which can be expressed as $D_g^2/(s^2 D_s)$ with the help of Eq. (56). Then, from Eq. (37), the average domain size at the crossover ℓ^* is on the order of $D_g/(sH_0)$.

The dynamics during the second stage depends on the probability distribution of domains of size η, $P_d(\eta)$ at time τ^*. For annihilating random walkers, which are a good approximation to domain boundaries during the first stage, Bramson and Griffeath [29] proved that $P_d(\eta)$ has exponential tail for large η of the form $e^{-\gamma\eta/\ell^*}$, where γ is a number of the order 1. Since each domain shrinks with velocity $2v_w$, the fraction of allele two can be expressed as

$$1 - F(t) \propto \int_0^\infty \eta e^{-\frac{\gamma(\eta + 2v_w t)}{\ell^*}} d\eta \propto e^{-\frac{\lambda s^2 D_s t}{D_g^2}}, \tag{57}$$

where λ is a number of order 1. From Eq. (57) it follows that, as in the well-mixed case, the selective sweep is exponentially fast, but the time constant of this process is proportional to s^{-2} rather than s^{-1}.

The analysis leading to Eq. (57) can be generalized to an arbitrary initial probability distribution, $P_d(\eta)$, provided the dynamics is dominated by selection and genetic drift. For example, if a population initially in equilibrium with respect to mutations and genetic drift (see Sec. V) is affected by an abrupt environmental change that makes allele one advantageous,

then the shift to the new equilibrium occurs exponentially fast with a time constant proportional to $\frac{sD_s^{1/2}\mu_{12}\mu_{21}}{D_g(\mu_{12}+\mu_{21})^{3/2}}$, assuming $P_d(\eta)$ has exponential tail of the form $e^{-\gamma'\eta/\ell}$, where γ' is a constant of order unity, and ℓ is given by Eq. (49).

We make two important observations based on the results of this section. First, the temporal dynamics of the one-dimensional stepping stone model with selection can depend strongly on the initial conditions. Second, the results in the weak selection limit are related to the results in the strong selection limit by the transformation $s \to s^2 D_s/D_g^2$ at least up to a numerical factor. The second observation suggests that, while data can be naively fitted to a well-mixed-population model, the fit in fact gives the "renormalized" value of s instead of the "bare" one.

VII. SIMULATIONS

In Secs. III, IV, V, and VI we reviewed and extended the theoretical analysis of the one-dimensional stepping stone model. This model, while of great theoretical interest, relies on a restrictive set of assumptions including large deme sizes and slow diffusive migration. The recent experiments by Hallatschek *et al.* [5], on the other hand, were carried out with bacterial fronts that were only a monolayer thick; therefore, demes consisted of only a few microbes. Moreover, depending on the microorganism, nearby demes can exchange a significant fraction of cells in each generation. In this section, we discuss numerical simulations not subject to these restrictions and compare them with the theoretical predictions.

We simulate L organisms arranged on a line and labeled by an integer l, $l = 1, 2, ..., L$. Each organism can be either of allelic type 1 or allelic type 2. During even generations, the offspring at site l comes from an organism at either site $l-1$ or site l, whereas, during odd generations it comes from either site l or $l+1$. The simulations embody the process illustrated in Fig. 2, laid out on a triangular lattice in space and time. Periodic boundary conditions are imposed at the left and right ends of the population. Let $12 \to 2$ refer to the event that the offspring has allelic type 2, while one of its possible parents has allelic type 1 and the other has allelic type 2, etc. The transition probabilities, which depend on the states of the possible ancestors, are then given by

$$
\begin{aligned}
11 \to 1: &\qquad 1-\tilde{\mu}_{12},\\
11 \to 2: &\qquad \tilde{\mu}_{12},\\
22 \to 1: &\qquad \tilde{\mu}_{21},\\
22 \to 2: &\qquad 1-\tilde{\mu}_{21},\\
12 \to 1: &\qquad \frac{1+\tilde{s}}{2}(1-\tilde{\mu}_{12})+\frac{1-\tilde{s}}{2}\tilde{\mu}_{21},\\
12 \to 2: &\qquad \frac{1+\tilde{s}}{2}\tilde{\mu}_{12}+\frac{1-\tilde{s}}{2}(1-\tilde{\mu}_{21}),\\
21 \to 1: &\qquad \frac{1+\tilde{s}}{2}(1-\tilde{\mu}_{12})+\frac{1-\tilde{s}}{2}\tilde{\mu}_{21},\\
21 \to 2: &\qquad \frac{1+\tilde{s}}{2}\tilde{\mu}_{12}+\frac{1-\tilde{s}}{2}(1-\tilde{\mu}_{21}).
\end{aligned}
\tag{58}
$$

The event $12 \to 2$ can happen either if allele one was selected for reproduction [probability $(1+\tilde{s})/2$] and it mutated (probability $\tilde{\mu}_{12}$) or if allele two was selected for reproduction [probability $(1-\tilde{s})/2$] and it did not mutate (probability $1-\tilde{\mu}_{21}$). Other transition probabilities are obtained analogously. Thus, the system we simulate is very similar to the voter model [12], equivalent to population genetics models with $N = 1$. However, to make the calculation faster, we use discrete generations rather than exponentially distributed waiting times until reproduction. We found no significant differences in dynamics between the voter model and the model used here.

First, we simulate the neutral model without mutations. To illustrate the similarities and differences between the one-dimensional stepping stone model and a growing population with an undulating front, we also simulate a flat population wave in a two-dimensional habitat; both are displayed in Fig. 2. Our model with an undulating front is the same as in Ref. [11], but we use a triangular grid instead of a cubic one. Figures 5 and 6 show how the average number of domain boundaries decrease with time; the insets show the mean square displacements of the boundaries as a function of time. The simulations confirm that the domain boundaries perform a diffusive random walk for the $(1+1)$-dimensional model with a flat front, but they move superdiffusively for the undulating front (Eden) model, in agreement with Ref. [11]. In this case, the number of domain boundaries decays faster for the undulating-front model compared to the $(1+1)$-dimensional flat front model that, as we show below, most closely tracks the prediction of the one-dimensional stepping stone model.

A single run of a simulation is shown in Fig. 7, and the spatial heterozygosity averaged

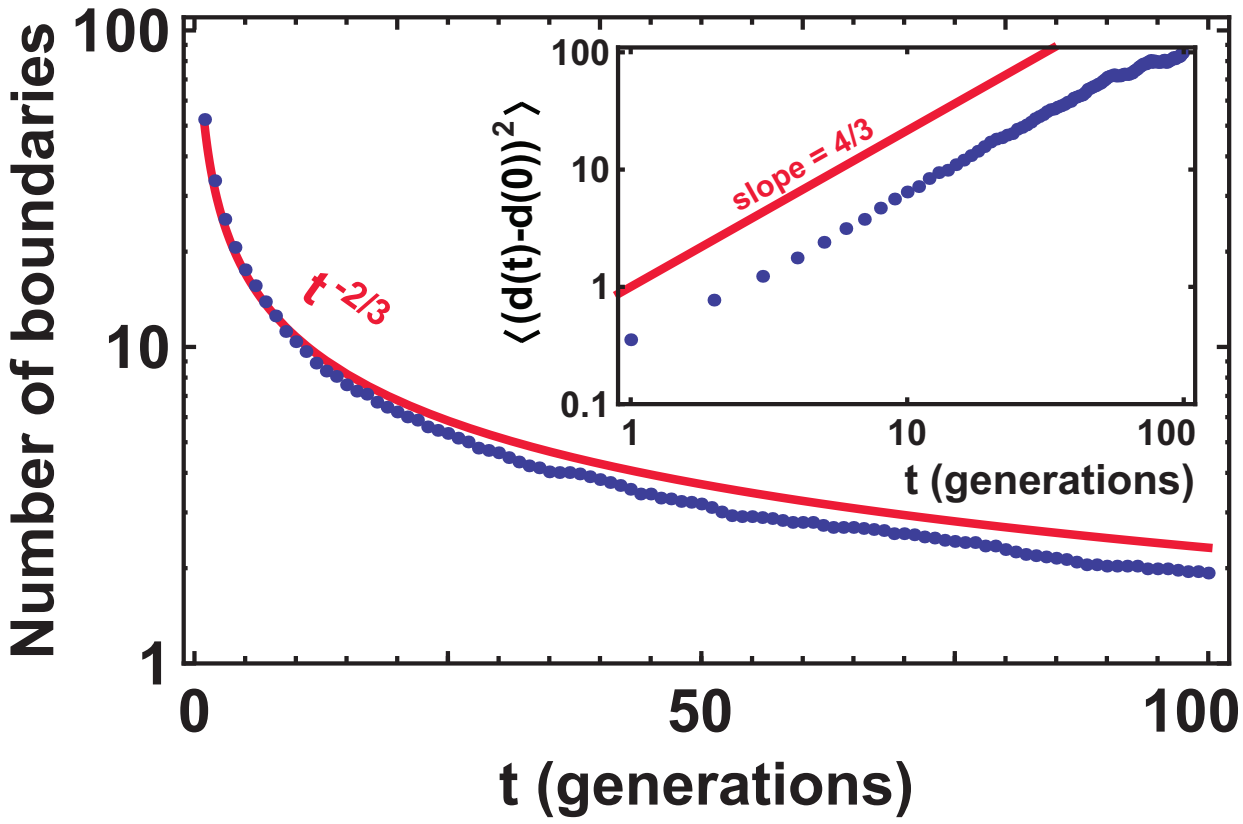

FIG. 5: (Color online) The number of monoallelic domain boundaries as a function of time in the undulating front model. The simulation of 100 demes averaged over 100 runs is plotted in blue (dots), and the theoretically expected decay of the number of boundaries as $t^{-2/3}$ (see Ref. [11]) is plotted in red (solid line). Inset: Log-log plot of the mean square displacement of monoallelic domain boundary end-points as a function of time in the same set of simulations as the main plot. The blue dots are the simulation data, and the solid red line is the expected slope according to Ref. [11].

many runs is shown in Fig. 8. Note that coarse-graining is required to properly represent the time evolution of $H(t, 0)$. Figure 9 shows that $H(t, x)$ for large t can be described well by the limiting shape of spatial heterozygosity given by Eq. (36). To properly represent $H(t, 0)$, we artificially define demes of a larger size by grouping M neighboring individuals into one deme. From a theoretical point of view, this procedure is similar to the formation of Kadanoff block spins as in renormalization group methods [30] whereas, from the point of view of population genetics, this procedure is similar to the methods of collecting data from a dispersed natural population. In field studies, scientists do not typically sample every

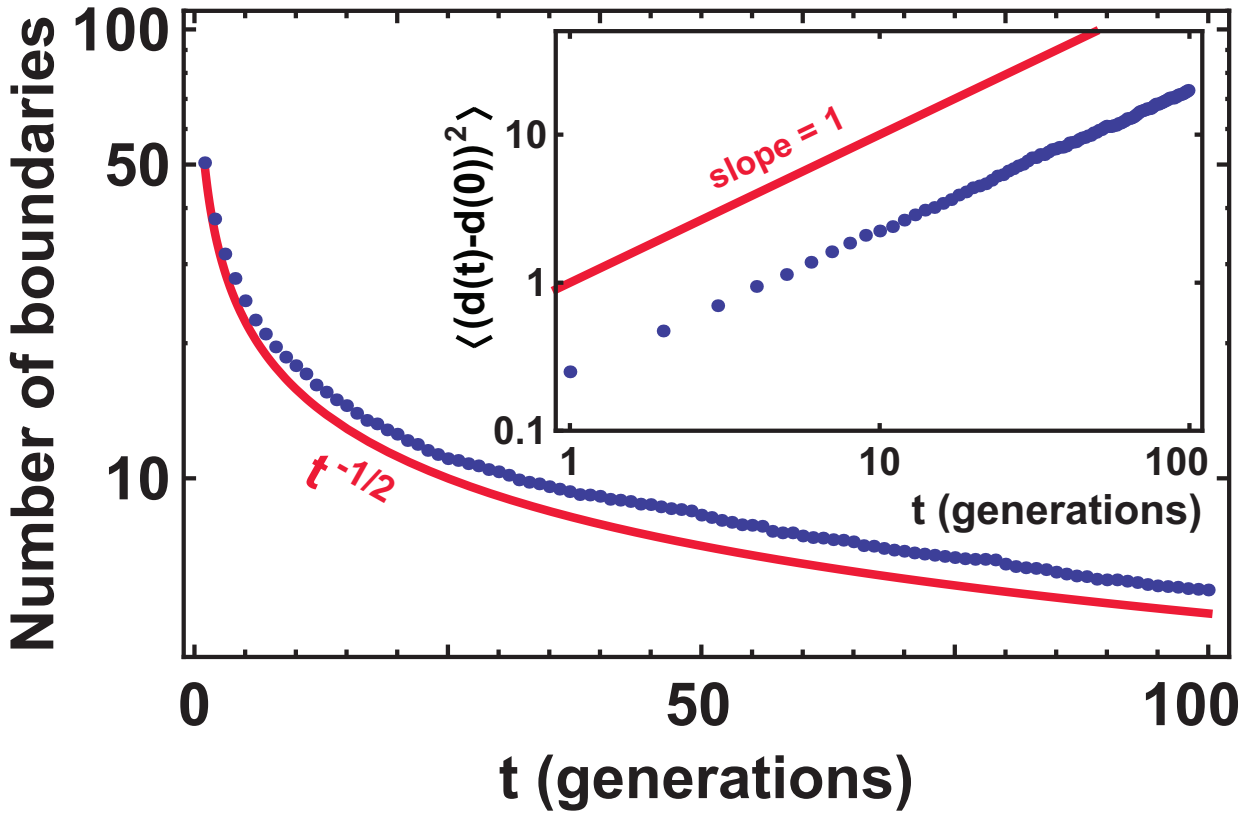

FIG. 6: (Color online) The number of monoallelic domain boundaries as a function of time in the flat front model. The simulation of 100 demes averaged over 100 runs is plotted in blue (dots), and the theoretically expected decay of the number of boundaries as $t^{-1/2}$ (see Ref. [26]) is plotted in red (solid line). Inset: Log-log plot of the mean square displacement of monoallelic domain boundary end-points as a function of time in the same set of simulations as the main plot. The blue dots are the simulation data, and the solid red line is the expected slope according to Ref. [16, 26] and Eq. (37).

single individual; instead, they often divide the habitat into patches and sample a representative number of individuals from those patches. To summarize, we keep the dynamics of the simulation exactly the same, but define the spatial heterozygosity on the demes of size M rather than on single individuals. We found that the local heterozygosity has the form $H(t,0) = \beta(M)t^{-1/2}$, as predicted by our analysis of the stepping stone model, for all M studied ($1 \leq M \leq 64$). From Eq. (35), we expect that $\beta \propto M^{-2}$; this expectation was also confirmed by our simulations.

As discussed in Sec. IV, the *total* fraction of allele one $\mathfrak{f}(t)$ fluctuates in an unusual way

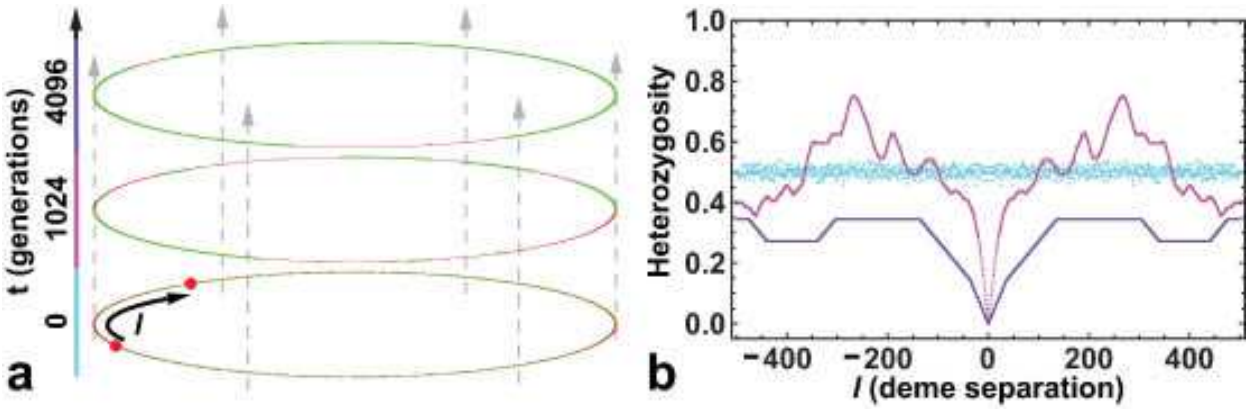

FIG. 7: (Color online) Simulation of microorganisms growing along a cylinder. (a) Cross sections of the cylinder at the inoculation time (bottom) and at two later times. The two genotypes are shown in red and green. Initially, both alleles are present in almost equal proportions, and the two later cross sections show the results of the coarsening process. (b) The spatially averaged heterozygosity [defined in the sense of Eq. (B1) but without taking the limit $L \to \infty$] for the three cross sections shown in a; the separation l is the shortest distance between two points around the cylinder. The colors correspond to the colors used is a. At inoculation, the heterozygosity fluctuates around 1/2 since the two phenotypes have equal probabilities of occupying any site. The only exception is the site $l = 0$, where the heterozygosity is zero automatically because we only allow a single microorganism per site. After 1024 generations short range correlations are clearly visible and after 4096 generations one can easily relate the features of the heterozygosity function to the sizes of the sectors in the corresponding cross section. The wiggles are eliminated when averaged over many realizations, as shown in Fig. 8.

with time. Figure 10a shows examples of these remarkable variable-step-length random walks. The fluctuations of $\mathfrak{f}(t)$ obey Eq. (43) and grow subdiffusively, as shown in Fig. 10b. We also find good agreement between the theory and the simulations in the presence of mutation for all values of M studied. Figure 11 shows the stationary spatial heterozygosity for $M = 1$. Finally, we studied selective sweeps in an initially well-mixed population. Figure 12a confirms the prediction from Eq. (57) that $F \propto (1-e^{-\alpha t})$, and Fig. 12b confirms the result of Sec. VI that, for strong genetic drift, the effective extinction rate α is proportional to s^2.

Numerical results for *three* neutral alleles are presented in Appendix E.

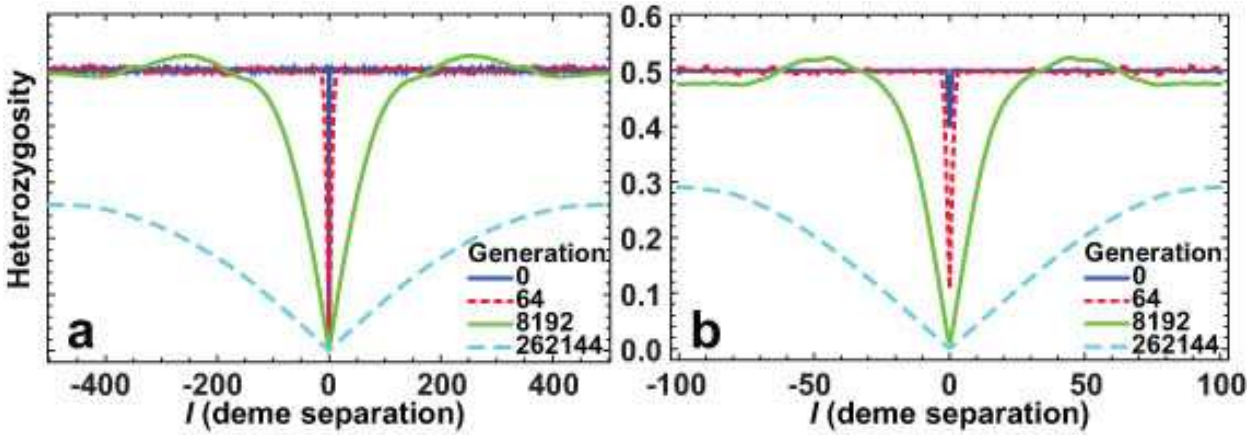

FIG. 8: (Color online) Effects of coarse-graining of the time evolution of the heterozygosity $H(t, l)$. The curves are averages of 100 model runs. (a) The $(1 + 1)$-dimensional model with a flat front, where each deme hosts only one organism. Consequently, the heterozygosity at $l = 0$ is zero at all times. Note the qualitative similarity to the analytical results at larger distances except for boundary effects. (b) Similar runs for the model except that the organisms have now been grouped into demes of size 5 before calculating the heterozygosity. This coarse-graining gives qualitative agreement with the analytical results even at $l = 0$.

VIII. CONCLUSIONS

Fluctuations due to sampling error during reproduction significantly affect the evolutionary dynamics of quasi one-dimensional populations, e.g. two-dimensional populations undergoing range expansions. These fluctuations lead to the genetic demixing illustrated in Fig. 13, where an initially well-mixed population of alleles "phase separates" into monoallelic domains. The transition is somewhat analogous to spinodal decomposition in physics and material science [31], but is also markedly different. In particular, unlike conventional demixing phase transitions in statistical mechanics, genetic demixing occurs only in a *low* number of spatial dimensions d ($d \leq 2$) [21, 31]. The dependence of genetic demixing on the number of spatial dimensions d is illustrated by the decay of local heterozygosity in the absence of selection and mutation. For long times, the functional form of the decay is given by [21],

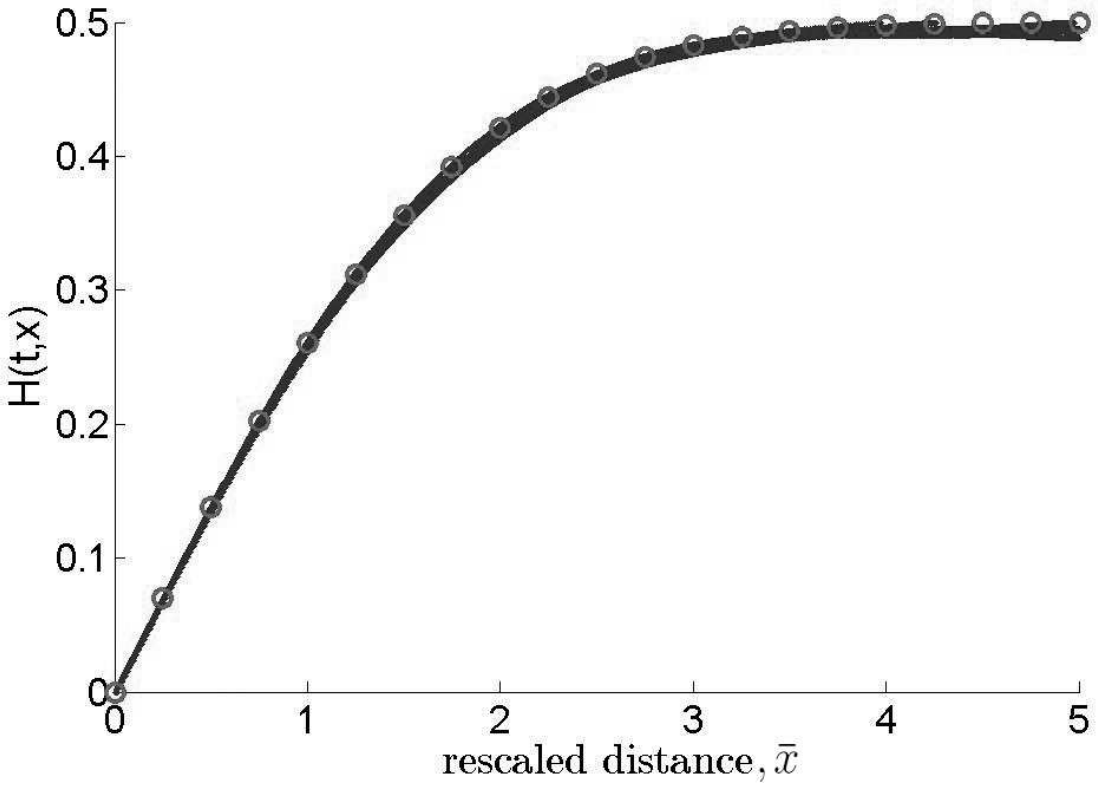

FIG. 9: Comparison between the analytical prediction for the limiting shape of $H(\infty, \bar{x})$ and the simulations with a flat population front. The continuous curve is formed by the data points representing $H(t, x)$ for several times between $t = 2 \cdot 10^4$ and $t = 4 \cdot 10^5$ plotted in the rescaled coordinates $\bar{x}$, and the circles represent the theoretical prediction of the limiting shape of the spatial heterozygosity, see Eq. (36). The data are obtained in a simulation of 3200 individuals for $4 \cdot 10^5$ generations with averaging over 500 realizations. At $t = 0$, each site was assigned either allele one or allele two with equal probability.

$$H(t,0) \sim \begin{cases} e^{-t/(2N\tau_g)} & d = 0, \\ (\tau_f/t)^{1/2} & d = 1, \\ 1/\ln(t) & d = 2, \\ \text{const} & d > 2. \end{cases} \tag{59}$$

Note that $d = 2$ is the critical dimension.

Here, we have shown that the one-dimensional stepping stone model has very different dynamics compared to the standard well-mixed-population models used in genetics. Most of

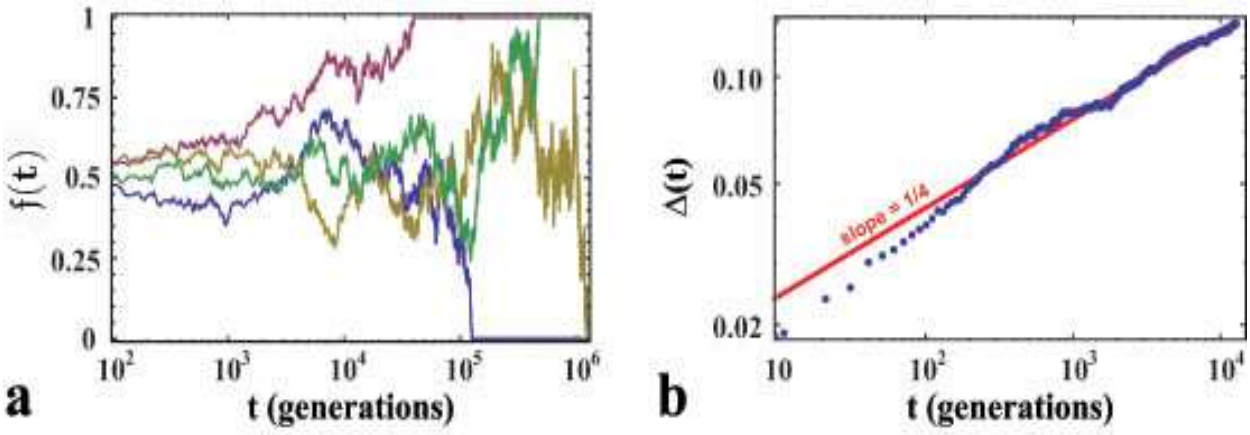

FIG. 10: (Color online) Genetic drift in a finite population. (a) The total fraction of allele one $\mathfrak{f}(t)$ versus time in four single runs of the neutral model with a flat front. Here $L = 1000$, and there are no mutations. (b) The standard deviation of the frequency of allele one $\Delta(t)$, shown with blue dots, is obtained from 220 realizations of the simulations described in a. The red solid line shows the slope expected from. Eq. (43).

the differences arise because, in the spatial model, populations segregate into monoallelic domains. As a result, genetic drift and selection can only act at the boundaries of the domains, which slows down the dynamics of the model. In particular, we found that, in the neutral model without mutation, fixation occurs exponentially fast in a well-mixed population, but the decay of heterozygosity is algebraic in the spatial model. Genetic drift in the population as a whole becomes weaker with time, as spatial diffusion causes the effective population size to increase. We also found that the standard deviation of the total fraction of one of the alleles (in the absence of selection and mutation) increases subdiffusively as $t^{1/4}$. Selective sweeps also occur more slowly in the spatial model: for weak selection, $s \ll D_g^2/D_s$, we found that the time constant of the selective sweep is quadratic in s in the spatial model, but it is only linear in s in the well-mixed-population model. The effects of mutation do not differ as dramatically in spatial and nonspatial models, but spatial stepping stone model reveals nontrivial spatial correlations and predicts a different value for the local steady state heterozygosity, proportional to $\sqrt{\mu_{12} + \mu_{21}}$ for small mutation rates, compared to $\mu_{12} + \mu_{21}$ in the well-mixed-population model.

Our main conclusion is that the data from natural populations may not always conform to the predictions of the well-mixed-population model and, even when it does, the estimated

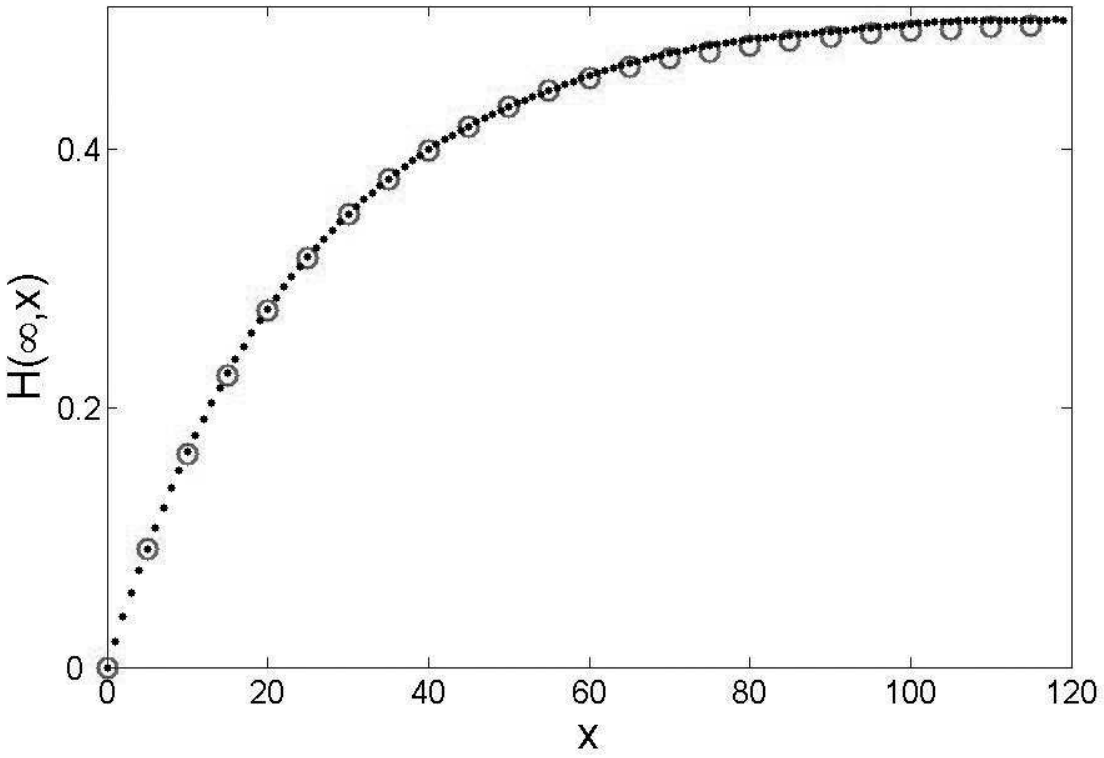

FIG. 11: Equilibrium between mutation and genetic drift in the absence of selection. Comparison between the analytical prediction for the steady state heterozygosity $H(\infty, x)$ and the simulations with $\tilde{\mu}_{12} = 10^{-4}$ and $\tilde{\mu}_{21} = \tilde{\mu}_{12}$. The dots represent the results of the simulation, and the circles represent the best fit of theoretical result given by Eq. (47) to the data. The data are obtained in a simulation of 3200 individuals for $2 \cdot 10^5$ generations with averaging over 100 realizations. At $t = 0$, each site was assigned either allele one or allele two with equal probability.

parameters from the model may not be biologically meaningful. The spatial model contains an important additional parameter, the spatial diffusion constant parameter D_s, which enters into many of the predictions. For example, the timescale for local fixation is given by D_s/D_g^2 rather than $N\tau_g$ [see Eq. (35)] and, for weak selective advantage, s is replaced by $s^2 D_s/D_g^2$, see Sec. VI. Moreover, as we saw in Sec. VII, the timescale of fixation depends on the partitioning of the population by the experimenter into measurement sites. Thus, care must be taken when interpreting the data from the natural populations. Finally, well-mixed-population models and experiments without spatial resolution do not account for spatial correlations, which contain important information about the population.

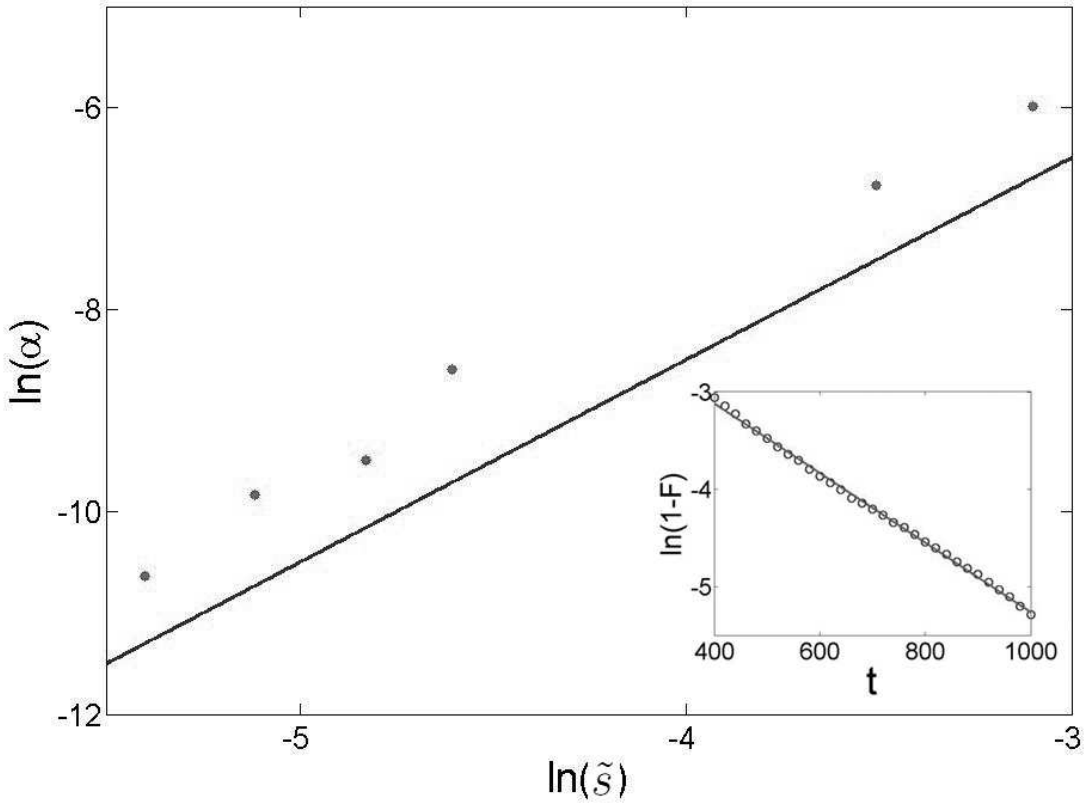

FIG. 12: The effective extinction rate α versus $\tilde{s}$ in the limit of weak selection. The dots are the data from the simulation, and the line has the slope equal to 2, that is the expected slope from Eq. (57). The data supports $\alpha \propto \tilde{s}^2$.The values of α are obtained from graphs like the one shown in the inset. Inset: $\ln(1-F)$ versus t for $\tilde{s} = 0.06$. The circles are the actual data points, and the line is the best least squares linear fit. The simulation confirms exponentially fast fixation. The data are obtained in a simulation of 1600 individuals for 6000 generations with averaging over 100 realizations. At $t = 0$, each site was assigned either allele one or allele two with equal probability.

Acknowledgments

M. A. is grateful for financial support from the Danish National Research Foundation through Center for Models of Life. Overall support for this project was provided by the National Science Foundation, through Grant DMR-0654191, a National Institute of General Medical Sciences Grant and the Harvard Materials Research Science and Engineering Center through DMR-0820484.

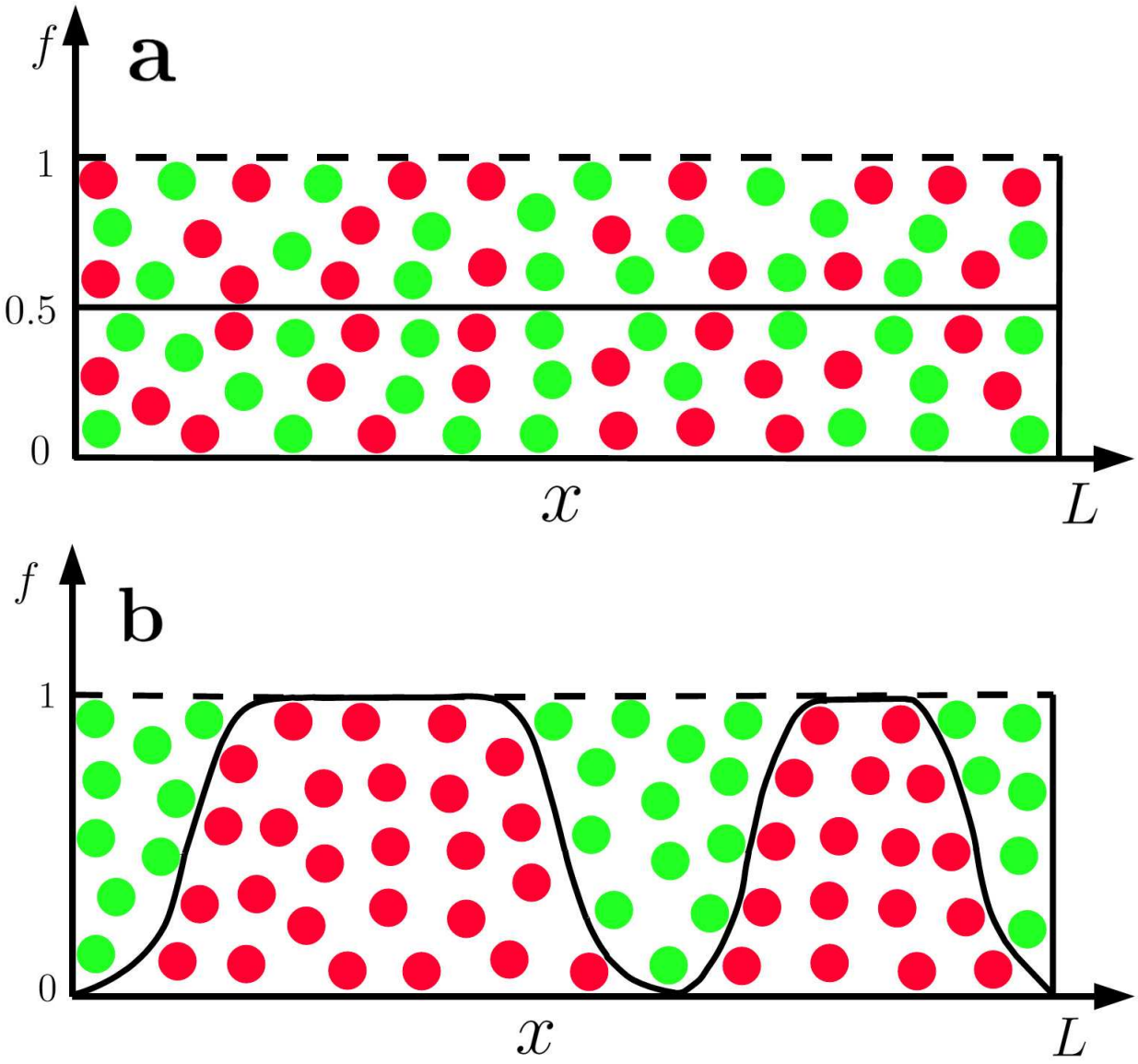

FIG. 13: (Color online) Illustration of spinodal-decomposition-like genetic demixing in a one-dimensional population. (a) Initially well-mixed population with red and green colors labeling different genotypes. (b) The same population several generations later. The frequency of one of the alleles is now oscillating between 0 and 1 because the population segregates into monoallelic domains.

APPENDIX A: SOLUTION OF THE NEUTRAL MODEL WITHOUT MUTATION

In this appendix, we solve Eq. (32) subject to initial condition $H(0,x) = H_0$. It is advantageous to first solve a simpler equation:

$$\frac{\partial}{\partial t}H = 2D_s\frac{\partial^2}{\partial x^2}H - b(t)\delta(x), \tag{A1}$$

where $b(t)$ is an arbitrary function of time. Equation (A1) is a standard diffusion equation with a sink term, and it can be readily solved in the Fourier domain. The result is

$$H(t,x) = H_0 - \int_0^t dt' \frac{b(t')e^{-\frac{x^2}{8D_s(t-t')}}}{\sqrt{8\pi D_s(t-t')}}. \tag{A2}$$

Note the convolution of $b(t')$ with the diffusion propagator. Now, we impose a self-consistency condition $b(t) = D_g H(t,0)$, which leads to

$$H(t,0) = H_0 - D_g\int_0^t dt' \frac{H(t',0)}{\sqrt{8\pi D_s(t-t')}}. \tag{A3}$$

This is Abel's integral equation of the second kind, canonically written as

$$y(x) + \lambda\int_a^x \frac{y(t)dt}{\sqrt{x-t}} = g(x), \tag{A4}$$

where $g(x)$ is a known function. The general solution of Eq. (A4) is given in Ref. [32], and it reads

$$\begin{aligned} y(x) &= G(x) + \pi\lambda^2\int_a^x e^{\pi\lambda^2(x-t)}G(t)dt, \quad \text{where} \\ G(x) &= g(x) - \lambda\int_a^x \frac{g(t)dt}{\sqrt{x-t}}. \end{aligned} \tag{A5}$$

Equations (33) and (34) follow from Eqs. (A2), (A3), (A4), and (A5).

APPENDIX B: AVERAGE DOMAIN DENSITY FROM THE SPATIAL HETEROZYGOSITY $H(t,x)$

In this appendix we derive the relationship between the spatial heterozygosity, $H(t,x)$, and the average domain density $n_d(t)$. From n_d, we can get a domain size by defining $\ell \equiv n_d^{-1}$.

The result for the domain density is valid for an arbitrary number of alleles, so in this appendix we use a broader definition of $H(x,t)$ as the average probability of sampling at time t two different alleles from two demes a distance x apart. We assume that the domains have formed, and they are on average much larger than the boundary regions.

Let $h(t,x_1,x_2)$ equal to 1 if both x_1 and x_2 are occupied by organisms in different allelic state and 0 otherwise. To compute ℓ, we use an alternative definition of $H(t,x)$ with ensemble average replaced by space average:

$$H(t,x)=\lim_{L\to\infty}\frac{1}{L}\int_0^L h(t,\xi,\xi+x)d\xi, \tag{B1}$$

where we assume periodic boundary conditions. Let us compute $H(t,x+\delta x)-H(t,x)=\lim_{L\to\infty}\frac{1}{L}\int_0^L[h(t,\xi,\xi+\delta x)-h(t,\xi,\xi)]d\xi$ for δx small compared to typical domain size but large compared to the deme spacing a. Now expand both sides in δx. At the lowest order in δx, each domain boundary contributes δx to the right hand side; therefore, $\frac{\partial}{\partial x}H(t,+0)$ equals the density of the domain boundaries. Upon defining the average domain size $\ell(t)$ as the inverse of the domain boundary density, we obtain the following relationship:

$$\ell(t)=\left(\frac{\partial H(t,+0)}{\partial x}\right)^{-1}. \tag{B2}$$

This relation is analogous to the one derived in Ref. [33].

We can further simplify Eq. (B2) by observing that

$$\frac{\partial H(t,+0)}{\partial x}=\frac{D_g H(t,0)}{4D_s}, \tag{B3}$$

which follows from integrating Eq. (31) or Eq. (C1) with respect to x from $-\epsilon$ to ϵ, $0<\epsilon\ll 1$, and noticing that $H(t,x)$ is an even function of x. The final result then reads

$$\ell(t)=\frac{4D_s}{D_g H(t,0)}. \tag{B4}$$

It should be emphasized that this result is only valid in the limit of very large domain sizes compared to the boundary regions, which means $H(t,0)\ll 1$. Therefore, the leading term in $H(t,0)$ is sufficient at this level of approximation. Note that Eqs. B2 and B4 are valid in the most general settings considered in this paper, i.e. in the presence of genetic drift, migration, selection, and mutation.

APPENDIX C: INFINITE ALLELES MODEL

In this appendix, we extend the analysis of the stepping stone model with mutations presented in Sec. V to the infinite alleles model. The infinite alleles model assumes that every new mutation creates a new allele, which is a good approximation for genes encoded by a large number of nucleotides because the number of all possible mutations is much larger than the number of all possible back mutations [17]. The equation of motion for $H(t,x)$, which we interpret as the average probability of sampling two different alleles from demes x apart, can be derived by following two lineages backward in time, as done in Sec. IV. In the presence of mutation, the right hand side of Eq. (32) should contain an additional term describing the rate of increase of $H(t,x)$ due to mutations in both of the lineages. Because, in the infinite alleles model, a mutation changes the probability that the organisms have different alleles from H to 1, that is by $1-H$, the new term is $2\mu(1-H)$, where μ is the mutation rate that is assumed to be the same for all types of mutations. Thus, Eq. (32) becomes

$$\frac{\partial}{\partial t}H = 2D_s\frac{\partial^2}{\partial x^2}H + 2\mu(1-H) - D_g H\delta(x) \tag{C1}$$

for the infinite alleles model (compare Eq. 46). The stationary solution of Eq. (C1) is given by

$$H(\infty,x) = 1 - \frac{e^{-\sqrt{\frac{\mu}{D_s}}|x|}}{1+\frac{1}{4}\sqrt{\frac{D_g^2}{D_s\mu}}}. \tag{C2}$$

At large separations, $H(\infty,x)$ approaches one, which is consistent with the infinite number of alleles. Locally, $H(\infty,0) = (1+\frac{1}{4}\sqrt{\frac{D_g^2}{D_s\mu}})^{-1}$, and if $H(\infty,0) \ll 1$ the population is segregated into domains containing only one allelic type. The average size of such domains follows from Eq. (B4):

$$\ell = \frac{4D_s}{D_g}\left(1+\frac{1}{4}\sqrt{\frac{D_g^2}{D_s\mu}}\right) \approx \sqrt{\frac{D_s}{\mu}}, \tag{C3}$$

where the last equality follows from the assumption that $H(\infty,0) \ll 1$. The approach to the stationary state can be either obtained by methods of Appendix A or by the change of variables $H(t,x) = H(\infty,t) + e^{-2\mu t}\hat{H}(t,x)$, which reduces Eq. (C1) to Eq. (32). The result is that the slowest decaying mode vanishes as $C\sqrt{\frac{D_s}{D_g^2 t}}e^{-2\mu t}$, where C is a constant.

The infinite allele model and Eq. (C1) has been analyzed before in Refs. [13, 24], where the stationary solution and the long time approach to the equilibrium were calculated. Our results are consistent with their findings.

APPENDIX D: THE ITÔ CALCULUS

In this appendix, we briefly discuss the Itô calculus. Our presentation relies on Refs. [19] and [22], which can be consulted for a more extensive presentation. For simplicity, we only consider nonspatial stochasic differential equations, but the results can be extended to spatial problems straightforwardly.

Let us analyze the following stochastic differential equation, which includes Eq. (20) as a special case,

$$\frac{d\psi}{dt} = \omega(\psi) + g(\psi)\Gamma(t), \tag{D1}$$

where $\Gamma(t)$ satisfies Eq. (21), and $\omega(\psi)$ and $g(\psi)$ are arbitrary continuously differentiable functions. From the point of view of ordinary calculus, Eq. (D1) is not well-defined because $\Gamma(t)$ is discontinuous at every point. One way to circumvent this problem is to use discrete time steps of infinitesimal length δt rather than continuous time. Then, Eq. (D1) takes the following form:

$$\frac{\psi(t+\delta t) - \psi(t)}{\delta t} = \omega[\psi(t)] + g[\psi(t)]\Gamma(t). \tag{D2}$$

However, this is not the only way to interpret Eq. (D1). For example, an alternative way to go from the continuous to a discrete description is to write Eq. (D1) as,

$$\frac{\psi(t+\delta t) - \psi(t)}{\delta t} = \omega\left[\frac{\psi(t) + \psi(t+\delta t)}{2}\right] + g\left[\frac{\psi(t) + \psi(t+\delta t)}{2}\right]\Gamma(t). \tag{D3}$$

In fact, there are an infinite number of ways to interpret Eq. (D1), depending on the relative weight of $\psi(t)$ and $\psi(t+\delta t)$ inside the arguments of the functions on the right hand side of the equation. The two most commonly used interpretations are Itô's and Stratonovich's prescriptions. The former corresponds to Eq. (D2), and the latter to Eq. (D3).

In physics, Stratonovich's prescription is commonly used because $\Gamma(t)$ is usually an approximation to a thermal noise with small but finite correlation time; therefore, the argument

of $g(\cdot)$ should be an average value of ψ over the time that the correlations persist. In population genetics, on the other hand, Ito's prescription is appropriate because a random change of the allele frequencies depends only on the genetic composition of the population *prior* to the change.

Without the stochastic term, Eqs. (D2) and (D3) would yield the same results provided δt is sufficiently small, but the stochastic terms remain different even in the limit $\delta t \to 0$. An easy way to see this difference is to average Eqs. (D2) and (D3) with respect to the nondifferentiable noise function $\Gamma(t)$. Itô's prescription gives $\langle \psi(t+\delta t)\rangle - \langle \psi(t)\rangle = \langle \omega[\psi(t)]\rangle \delta t$ because $\langle g[\psi(t)]\Gamma(t)\rangle = \langle g[\psi(t)]\rangle\langle \Gamma(t)\rangle = 0$ due to the independence of $\psi(t)$ and $\Gamma(t)$. A similar simplification, however, cannot be applied to Stratonovich's prescription because, generically, the stochastic term depends on $\psi(t+\delta t)$, which is not independent of $\Gamma(t)$.

Because of the aforementioned ambiguity of the stochastic differential equations with multiplicative noise in the continuous time limit, care must be taken while differentiating stochastic variables. While the rules of ordinary calculus apply to Stratonovich's prescription, special rules of the Itô calculus are required for Itô's prescription when tracking the evolution of, say, a polynomial function $u[\psi(t)]$ of the stochastic variable obeying Eq. (D1). In this paper, we use Itô's formula, namely [19, 22]

$$\frac{d}{dt}u[\psi(t)] = u'[\psi(t)]\omega[\psi(t)] + u'[\psi(t)]g[\psi(t)]\Gamma(t) + \frac{1}{2}u''[\psi(t)]g^2[\psi(t)], \tag{D4}$$

where $u(\psi)$ is a twice continuously differentiable function, and the primes now indicate differentiation with respect to ψ.

APPENDIX E: A MODEL WITH SEVERAL NEUTRAL ALLELES

A model with q neutral alleles is an intermediate case between the two-alleles model that we focus on in this paper and the infinite alleles model discussed in Appendix C. The q-alleles model is also analogous to nonequilibrium q-state Potts models. In this appendix, we briefly outline how the q-alleles model can be formulated and solved in the language of one and two-point correlation functions, compare our analytical predictions to simulations, and extend Eq. (43) to the undulating front model.

To specify the q-alleles model, we let $f_i(t,x)$ be the frequency of allele i at time t and position x; these quantities satisfy $\sum_{i=1}^{q} f_i(t,x) = 1$. The spatial diffusion and coalescence

probability of two lineages are still characterized by D_s and D_g respectively. Intra-allelic mutations are described by the mutation matrix μ_{ij}, which is the probability of allele i mutating into allele j if $i \neq j$. When $i = j$, we let $\mu_{ii} = -\sum_{j=1,\, j\neq i}^{q} \mu_{ij}$ to describe the outflow of alleles from allelic state i due to mutations.

The dynamics of the q-alleles model can be analyzed by considering one-point correlation functions $F_i(t,x) = \langle f_i(t,x)\rangle$ and two-point correlation functions $F_{ij}(t,x_1,x_2) = \langle f_i(t,x_1) f_j(t,x_2)\rangle$. $F_i(t,x)$ is the probability to find allele i at position x at time t, and $F_{ij}(t,x_1,x_2)$ is the probability to simultaneously find at time t allele i at position x_1 and allele j at position x_2. The evolution equations for these correlation functions are obtained by tracing one and two lineages backward in time; the results are

$$\frac{\partial F_i(t,x)}{\partial t} = D_s \frac{\partial^2 F_i(t,x)}{\partial x^2} + \sum_{j=1}^{q} \mu_{ji} F_j(t,x), \tag{E1}$$

$$\begin{aligned}\frac{\partial F_{ij}(t,x_1,x_2)}{\partial t} =& D_s \left(\frac{\partial^2}{\partial x_1^2} + \frac{\partial^2}{\partial x_2^2}\right) F_{ij}(t,x_1,x_2) + D_g \delta(x_1-x_2)[\delta_{ij} F_i(t,x_1) - F_{ij}(t,x_1,x_2)] + \\ & \sum_{i'=1}^{q}\sum_{j'=1}^{q} [\mu_{i'i} F_{i'j}(t,x_1,x_2) + \mu_{j'j} F_{ij'}(t,x_1,x_2)],\end{aligned} \tag{E2}$$

where δ_{ij} is Kronecker's delta, which is zero if $i \neq j$ and one otherwise. Thus, for a generic mutation matrix μ_{ij} one has to solve a system of coupled linear partial differential equations.

For simplicity and the ease of comparison with the other results in this paper, let us assume spatial homogeneity and identical mutation rates between any two alleles, $\mu_{i\neq j} = \mu/q$. Under these assumptions, Eq. (E2) can be simplified by introducing averaged spatial heterozygosity

$$H(t,x) = \sum_{i=1}^{q} \sum_{\substack{j=1 \\ j\neq i}}^{q} F_{ij}(t,0,x) = \sum_{i=1}^{q} \langle f_i(t,0)[1 - f_i(t,x)]\rangle, \tag{E3}$$

which is the probability to sample two different alleles at time t distance x apart. The equation of motion for $H(t,x)$ can be derived both from Eq. (E2) and, more simply, by tracing two lineages backward in time:

$$\frac{\partial}{\partial t} H = 2D_s \frac{\partial^2}{\partial x^2} H + 2\mu \left(\frac{q-1}{q} - H\right) - D_g H \delta(x). \tag{E4}$$

Note that Eq. (E4) agrees with Eq. (C1) in the limit $q \to \infty$ and with Eq. (46) for $\mu_{12} = \mu_{21} = \mu/2$. Since Eq. (E4) has the same functional form as Eq. (C1), the methods of Appendix C can be used to solve for $H(t, x)$.

In the absence of mutations, Eq. (E4) is identical to Eq. (32), as we briefly mentioned in Sec. IV. However, q-alleles models with different q may have slightly different dynamics due to q-dependent initial conditions: for example, an initially well-mixed population is represented by $H(0, x) = H_0 = 1 - 1/q$. Thus, the results of Sec. IV apply to the q-alleles model, provided appropriate initial conditions are used. In particular, we expect the standard deviation of $\mathfrak{f}_i(t)$, the total frequency of allele i, in a finite population to grow as $t^{1/4}$. This is indeed confirmed by our simulations shown in Fig. 14. Spatial correlations in the nonequilibrium q-state Potts model have recently been analyzed by Masser and ben-Avraham [34], who also found that two-point correlation functions obey the same q-independent equation of motion.

Finally, one can obtain the behavior of the standard deviation of the total frequency of allele one, $\Delta(t)$, in the undulating front model by the following scaling argument. We consider $\Delta(t)$ at large times after monoallelic domains have formed. Let $N_d(t)$ be the number of domains consisting of allele one and $d_k(t),\ k = 1, 2, ..., N_d(t)$ be lengths of these domains. Then, $\Delta(t)$ is given by

$$\Delta(t) = \frac{1}{L^2} \left\langle \left[\sum_{k=1}^{N_d(t)} d_k(t) - \langle \sum_{k=1}^{N_d(t)} d_k(t) \rangle \right]^2 \right\rangle . \tag{E5}$$

We simplify Eq. (E5) by making an approximation that $N_d(t)$ and $d_k(t)$ for $k = 1, 2, ..., N_d(t)$ are independent random variables, which gives

$$\Delta(t) \approx \frac{1}{L^2} \left\{ \langle N_d(t) \rangle [\langle d_1^2(t) \rangle - \langle d_1(t) \rangle^2] + \langle d_1(t) \rangle^2 [\langle N_d^2(t) \rangle - \langle N_d(t) \rangle^2] \right\} , \tag{E6}$$

where we used the fact that $d_i(t)$ are identically distributed.

By using first passage time analysis discussed in Ref. [35], one can show that $\langle N_d^2(t) \rangle - \langle N_d(t) \rangle^2 \propto \langle N_d(t) \rangle [\langle d_1^2(t) \rangle - \langle d_1(t) \rangle^2] / \langle d_1(t) \rangle^2 \propto L[\langle d_1^2(t) \rangle - \langle d_1(t) \rangle^2] / \langle d_1(t) \rangle^3$. Thus,

$$\Delta(t) \propto \frac{1}{L \langle d_1(t) \rangle} [\langle d_1^2(t) \rangle - \langle d_1(t) \rangle^2]. \tag{E7}$$

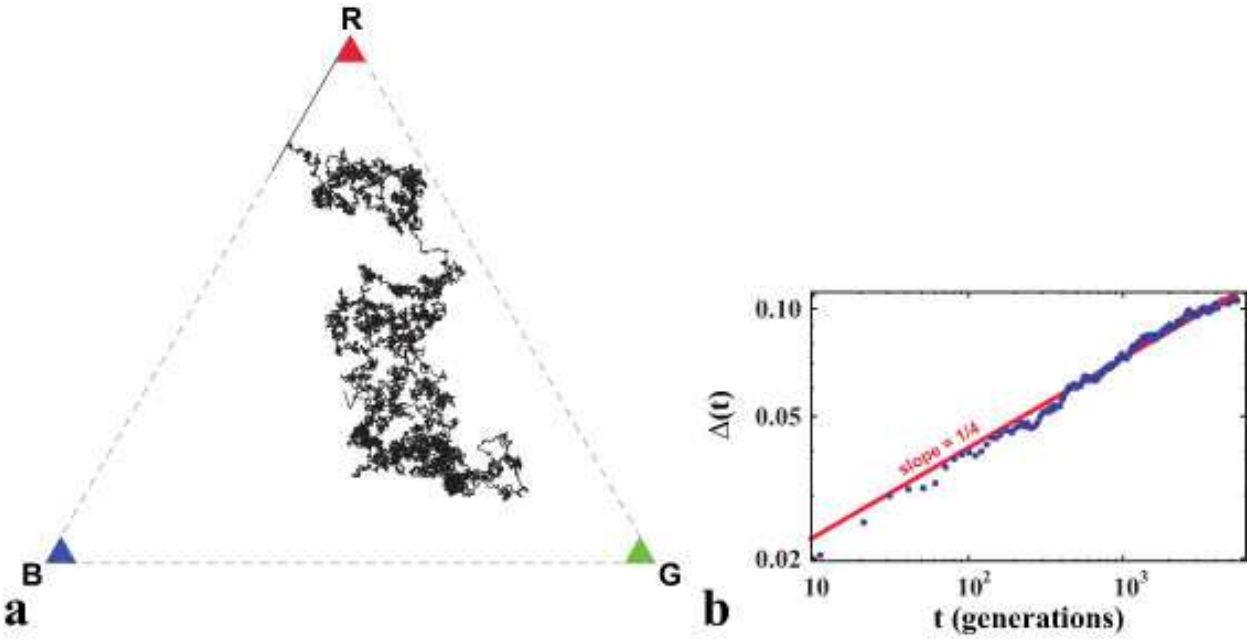

FIG. 14: (Color online) Genetic drift in a finite population with three alleles. (a) The genetic composition of the population $[\mathfrak{f}_1(t), \mathfrak{f}_2(t), \mathfrak{f}_3(t)]$ projected on the plane $\sum_{i=1}^{3} \mathfrak{f}_i(t) = 1$ in a single run of the neutral 3-alleles model with a flat front. Here $L = 1000$, and there are no mutations. (b) The standard deviation of the frequency of allele one $\Delta(t)$, shown with blue dots, is obtained from 110 realizations of the simulations described in a. The red solid line shows the slope expected from Eq. (43).

Upon recalling, that, in the undulating front model, $\langle d_1(t) \rangle \propto t^{\zeta}$, and $\langle d_1(t) \rangle^2 \propto t^{2\zeta}$, we conclude that

$$\Delta(t) \propto \frac{t^{\zeta}}{L} \propto \frac{t^{2/3}}{L}, \tag{E8}$$

where, in the last proportionality, we used $\zeta = 2/3$ from Ref. [11].

---

[1] E. Mayr, *Systematics and the origin of species from the viewpoint of a zoologist* (New York: Columbia University Press, 1942).

[2] S. Ramachandran, O. Deshpande, C. Roseman, N. Rosenberg, M. Feldman, and L. Cavalli-Sforza, Proceedings of the National Academy of Sciences **102**, 15942 (2005).

[3] A. Templeton, Nature **416**, 45 (2002).

[4] G. Hewitt, Biological Journal of the Linnean Society **58**, 247 (1996).

[5] O. Hallatschek, P. Hersen, S. Ramanathan, and D. R. Nelson, Proceedings of the National Academy of Sciences **104**, 19926 (2007).

[6] M. Kimura and G. Weiss, Genetics **49**, 561 (1964).

[7] S. Wright, Genetics **28**, 114 (1943).

[8] G. Malécot, Cold Springs Harbor Symp. Quant. Biol **20**, 52 (1955).

[9] R. Fisher, Ann. Eugenics **7**, 353 (1937).

[10] A. Kolmogorov, N. Petrovsky, and N. Piscounov, Moscow University Bulletin of Mathematics **1**, 1 (1937).

[11] Y. Saito and H. Müller-Krumbhaar, Physical Review Letters **74**, 4325 (1995).

[12] J. Cox and D. Griffeath, Ann. Probab. **14**, 347 (1986; for a recent review of voter models, see T. M. Liggett, *Interacting Particle Systems* (Springer, 2005)).

[13] G. Malécot, Theor. Popul. Biol. **8**, 212 (1975).

[14] N. Barton, F. Depaulis, and A. Etheridge, Theoretical Population Biology **61**, 31 (2002).

[15] B. Houchmandzadeh and M. Vallade, Physical Review E **68**, 61912 (2003).

[16] M. Bramson and J. Lebowitz, Journal of Statistical Physics **62**, 297 (1991).

[17] D. Hartl and A. Clark, *Principles of population genetics* (Sunderland, Sinauer Associates, 1989).

[18] J. Crow and M. Kimura, *An Introduction to Population Genetics Theory* (1970).

[19] H. Risken, *The Fokker-Planck equation: Methods of Solution and Applications* (Springer-Verlag Berlin and Heidelberg GmbH & Co. K, 1989).

[20] M. Kimura, Proceedings of the National Academy of Sciences **41**, 144 (1955).

[21] T. L. Duty, PhD in Physics, The University of British Columbia, Department of Physics and Astronomy, Department of Physics and Astronomy, The University of British Columbia, 6224 Agricultural Road Vancouver, B.C., Canada V6T 1Z1 (2000).

[22] C. Gardiner, *Handbook of Stochastic Methods* (Springer New York, 1985).

[23] S. Wright, Genetics **16**, 97 (1931).

[24] T. Nagylaki, Proceedings of the National Academy of Sciences of the United States of America **71**, 2932 (1974).

[25] T. Nagylaki, Proceedings of the National Academy of Sciences of the United States of America **75**, 423 (1978).

[26] O. Hallatschek and D. R. Nelson, http://arXiv.org/abs/0810.0053 (2008).

[27] J. Lin, Physical Review A **44**, 6706 (1991).

[28] C. Doering, C. Mueller, and P. Smereka, Physica A **325**, 243 (2003).

[29] M. Bramson and D. Griffeath, Ann. Probab **8**, 183 (1980).

[30] G. Ódor, Reviews of Modern Physics **76**, 633 (2004).

[31] M. Scheucher and H. Spohn, Journal of Statistical Physics **53**, 279 (1988).

[32] A. Polyanin and A. Manzhirov, *Handbook of Integral Equations* (CRC Press, 1998).

[33] D. Ben-Avraham, Physical Review Letters **81**, 4756 (1998).

[34] T. Masser and D. ben Avraham, Physics Letters A **275**, 382 (2000).

[35] S. Redner, *A guide to first passage time processes* (Cambridge University Press, 2001).